AD-A073 825 MASSACHUSETTS INST OF TECH CAMBRIDGE AEROPHYSICS LAB F/G 20/4
WAKE STUDIES RELATED TO REENTRANT PYRAMIDS.(U)
AUG 79 M SOLOMON, M FINSTON, C W HALDEMAN F44620-76-C-0049
UNCLASSIFIED MIT-TR-205 AFOSR-TR-79-0984 NL

1 OF 1
AD A073825

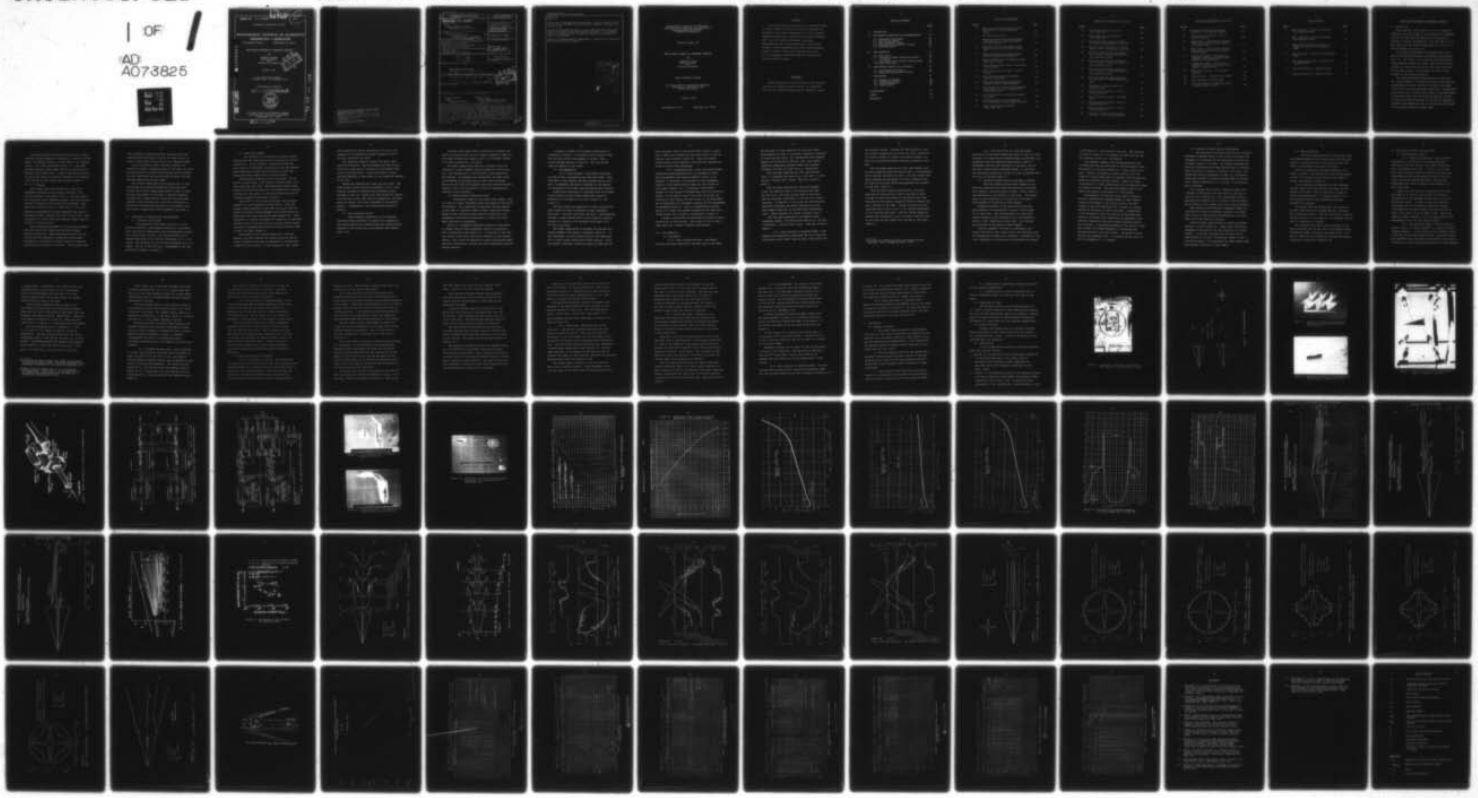

END
DATE FILMED
10-79
DDC

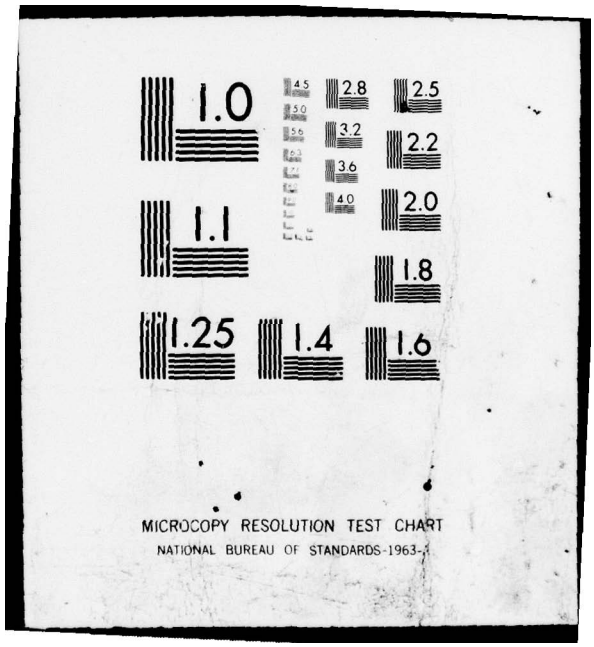
1.0
1.1
1.25
1.4
1.6
1.8
2.0
2.2
2.5
2.8
3.2
3.6
4.0
4.5
5.0
5.6
MICROCOPY RESOLUTION TEST CHART
NATIONAL BUREAU OF STANDARDS-1963-A

AFOSR-TR- 79-0984

LEVEL II

Aerophysics Laboratory TR 205

MASSACHUSETTS INSTITUTE OF TECHNOLOGY
AEROPHYSICS LABORATORY

560 Memorial Drive Cambridge, Ma. 02139

WAKE STUDIES RELATED TO REENTRANT PYRAMIDS

by

Marshall Solomon
Morton Finston
and
Charles W. Haldeman

August, 1979

Final Scientific Report
1 January 1976 - 30 November 1978

Distribution Unlimited

ORIGINAL CONTAINS COLOR PLATES: ALL DDC REPRODUCTIONS WILL BE IN BLACK AND WHITE.

AIR FORCE OFFICE OF SCIENTIFIC RESEARCH
Building 410, Bolling Air Force Base
Washington, D.C. 20332

Approved for public release;
distribution unlimited.

AIR FORCE OFFICE OF SCIENTIFIC RESEARCH (AFSC)
NOTICE OF TRANSMITTAL TO DDC
This technical report has been reviewed and is approved for public release IAW AFR 190-12 (7b).
Distribution is unlimited.
A. D. BLOSE
Technical Information Officer

Unclassified

SECURITY CLASSIFICATION OF THIS PAGE (When Data Entered)

REPORT DOCUMENTATION PAGE	READ INSTRUCTIONS BEFORE COMPLETING FORM
1. REPORT NUMBER (12) (14) AFOSR-TR-79-0984 / 2. GOVT ACCESSION NO.	3. RECIPIENT'S CATALOG NUMBER
4. TITLE (and Subtitle) (6) WAKE STUDIES RELATED TO REENTRANT PYRAMIDS	5. TYPE OF REPORT & PERIOD COVERED Final Scientific 1/1/76 - 11/30/78
	6. PERFORMING ORG. REPORT NUMBER (14) MIT-TR-205
7. AUTHOR(s) (10) Marshall Solomon, Morton Finston and Charles W. Haldeman	8. CONTRACT OR GRANT NUMBER(s) (15) F44620-76-C-0049
9. PERFORMING ORGANIZATION NAME AND ADDRESS Massachusetts Institute of Technology Aerophysics Laboratory Cambridge, Massachusetts 02139	10. PROGRAM ELEMENT, PROJECT, TASK AREA & WORK UNIT NUMBERS
11. CONTROLLING OFFICE NAME AND ADDRESS Air Force Office of Scientific Research Building 410 Bolling AFB, D.C. 20332	12. (11) REPORT DATE August, 1979 / 13. NUMBER OF PAGES 78
14. MONITORING AGENCY NAME & ADDRESS (if different from Controlling Office) (12) 81 p.	15. SECURITY CLASS. (of this report) Unclassified / 15a. DECLASSIFICATION/DOWNGRADING SCHEDULE
16. DISTRIBUTION STATEMENT (of this Report) Distribution Unlimited (9) Final rept.	
17. DISTRIBUTION STATEMENT (of the abstract entered in Block 20, if different from Report) 1 Jan 76 - 30 Nov 78,	
18. SUPPLEMENTARY NOTES	
19. KEY WORDS (Continue on reverse side if necessary and identify by block number) Ground Testing, Wake, Reentrant Pyramid, Maikapar Body, Magnetic Model Suspension, Supersonic Aerodynamics	

DDC RECEIVED SEP 17 1979 C

20. ABSTRACT (Continue on reverse side if necessary and identify by block number)

Measurements of pitot pressure in the near wake of a magnetically-supported pyramid body 2 inches long having a 4-point star-shaped base are reported at M=6.32 and Re_L=99,000. Most data was obtained at conditions giving 0.8=χ, the hypersonic viscous interaction parameter. Under these conditions the bow shock is attached to the external ribs (15° half angle) of the pyramid and has a nearly circular shape at 0.28 spans downstream of the base. Wake surveys indicated that the rear stagnation point is closer than 0.28 base

DD FORM 1 JAN 73 1473 ØØ92ØØ Unclassified

SECURITY CLASSIFICATION OF THIS PAGE (When Data Entered)

BLOCK #20
cont...

spans and no wake shock was detectable. Drag measurements from Re_L=74,000 to 247,000 revealed a strong decrease in C_D with increase in Re.

Benchmark measurements behind a wire-supported model indicated gross interference with wake pressure profiles. A 310 percent increase in base pressure compared to magnetically-supported models was observed.

Results indicated magnetic suspension is mandatory for meaningful measurements with this shape.

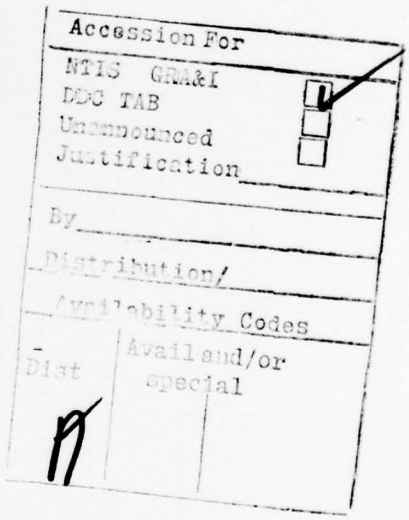

Massachusetts Institute of Technology
Department of Aeronautics and Astronautics
Aerospace Research Division
Aerophysics Laboratory

Technical Report 205

WAKE STUDIES RELATED TO REENTRANT PYRAMIDS

by

Marshall Solomon
Morton Finston
and
Charles W. Haldeman

FINAL SCIENTIFIC REPORT

Air Force Office of Scientific Research
Contract No. F44620-76-C-0049
MIT OSP No. 83632

August, 1979

560 Memorial Drive Cambridge, Ma. 02139

FOREWORD

This investigation was sponsored by the United States Air Force, Office of Scientific Research, Building 410, Bolling Air Force Base, Washington, D.C. under Contract F44620-76-C-0049 from 1 January 1976 through 30 November 1978. M.I.T.'s Lincoln Laboratory, Lexington, Massachusetts, was a joint sponsor during the period October 1, 1975 through April 30, 1976, under Purchase Order No. CC-614. The work was carried out at the M.I.T. Aerophysics Laboratory under the direction of Professor Morton Finston.

PERSONNEL

Technical personnel who contributed to the reported research are Professor Morton Finston, Dr. Charles W. Haldeman, Mr. Marshall Solomon and Mr. Charles E. Hawks.

TABLE OF CONTENTS

LIST OF ILLUSTRATIONS

LIST OF ILLUSTRATIONS (continued)

LIST OF ILLUSTRATIONS (concluded)

LIST OF TABLES

WAKE STUDIES RELATED TO REENTRANT PYRAMIDS

I. Introduction

During the past several years the M.I.T. Aerophysics Laboratory has been engaged in the experimental investigation of the supersonic and hypersonic near wakes of a variety of reentry configurations. The near wake of a 7^{o} half angle cone was studied by McLaughlin (1) at $M_{\infty} = 4.3$ and by Blankson (2) at $M_{\infty} = 6.3$.

The present investigation is concerned with the reentrant pyramid configuration, also known as the Maikapar body (3). This body is one of the few three-dimensional, non-axisymmetric shapes for which, under certain circumstances, an analytical solution for the flow field ahead of the base is known. This accounts for much of the interest in the reentrant pyramid.

The reentrant pyramid configuration is derived by the "inverse method" (4) wherein the walls of the body are constructed from stream surfaces of a known flow field, in this case inviscid, supersonic wedge flow. Consequently, these bodies have a "design point" which is the Mach number of the known flow field from which the body was derived. On design, the flow field ahead of the base is composed of regions of two-dimensional flow with plane shocks attached to and spanning adjacent leading edges.

The present effort has been concentrated on a single reentrant pyramid geometry of dimensions: external rib half angle = 15 degrees, internal rib half angle = 2.40 degrees, length = 2.00 inches and number of fins = 4. The plane spanning adjacent leading edges lies at an angle of 10.73 degrees to the model's axis. A shock inclined to the free stream by this angle will deflect streamlines 2.40 degrees (the internal rib half angle) when the Mach number is $M_\infty = 6.3 = M_{design}$.

Wind tunnel tests were carried out in the M.I.T. Aerophysics Laboratory's Gas Dynamics Facility. This facility combines a continuous flow $M_\infty = 6.32$ wind tunnel with a magnetic model suspension system. The wind tunnel's reservoir temperature and pressure are adjustable. Most tests were carried out at $T_o = 470^oF$ and $P_o = 40.0$ psia. Additional measurements were made throughout the tunnel's stagnation pressure range of 30.0 psia to 100.0 psia. This corresponds to a free stream unit Reynolds number range of 37,000 to 124,000 per inch.

Pitot pressure measurements in the reentrant pyramid near wake covered the region from the base to three diameters downstream. These measurements consist of continuous profiles produced by traversing a pitot probe horizontally, vertically or axially through the wake and recording pitot pressure vs. position. Pitot pressure was

also recorded at several stagnation pressures while the probe was held stationary, close to the model's base, in order to obtain data on base pressure vs. Reynolds number.

Using the magnetic model suspension system it is possible to measure aerodynamic drag at zero angle of attack by calibrating the current flowing through the drag magnet. The drag coefficient has been measured throughout the unit Reynolds number range of the tunnel.

The original objectives of this project were to completely map the reentrant pyramid near wake with pitot pressure and recovery temperature probes in order to study the axial development of the wake's azimuthal asymmetry. Although only a modest amount of data has been collected, compared to our original goal, sufficient information is available to identify most features of the pyramid's wake and to make a comparison to the axisymmetric cone wake.

II. Experimental Techniques and Instrumentation

2.1 Hypersonic Wind Tunnel

The hypersonic wind tunnel at the M.I.T. Aerophysics Laboratory's Gas Dynamics Facility is a continuous flow, open-circuit design with fixed interchangeable nozzles and a free jet test section. The nozzle used here has a nominal Mach number of 6.3 and exit dimensions of 5.1 x 3.1 inches. The inviscid core of the free jet measures 4.1 x 2.2 inches. Dry air is the test gas. A photograph of the test section bell appears in Figure 1.

2.2 Wind Tunnel Models

The selection of a particular reentrant pyramid configuration for wind tunnel testing was based on several criteria (5). These included: compatibility with the wind tunnel jet dimensions, compatibility with the magnetic model suspension system's optical position sensor and a design point Mach number at the test Mach number.

The dimensions selected on this basis were: 15^{o} external rib half angle, 2.40^{o} internal rib half angle, 2.00 inch length and four fins. These dimensions yield a base diameter (external rib span) of 1.072 inches and an internal rib span of 0.168 inches. A three-view drawing of the 15^{o} reentrant pyramid is presented in Figure 2.

Unlike the 7^{o} cones tested previously, the reentrant pyramid is a non-axisymmetric configuration. Since the magnetic model suspension system does not control the roll degree of freedom, various methods of roll control were incorporated into early wind tunnel model designs (5). These consisted of a variety of schemes for weighting or lightening different fins so that the center of gravity would be below the center of magnetization and gravity would hold the model at zero roll angle (Figure 3).

This method of roll control worked well, wind-off. However, the offset between the center of gravity and the center of magnetization made it impossible to suspend such a model with the wind-on. It was necessary to use a model

with a symmetrical weight distribution and rely on the asymmetry of the suspension system's magnetic field to provide a preferred roll angle.

This approach produced a stable roll angle, both wind-off and wind-on. The only penalty was that the preferred roll angle was not necessarily zero degrees (fins vertical and horizontal), varying from model to model, and also dependent to some extent on the stagnation pressure of the flow.

Models were machined from ingot iron bar stock. The model design finally settled on included a 0.25" x 0.08" diameter cylindrical samarium cobalt permanent magnet embedded in each fin. Models were also drilled out axially from the base so that they could be slipped over the pitot probe for support until being suspended by the magnetic balance. A photograph of this model design appears in Figure 4.

2.3 Wire Suspension System

Before magnetic suspension of the reentrant pyramid had been perfected, an apparatus for supporting wind tunnel models with tungsten wires was constructed and employed in the acquisition of preliminary wake measurements (5,6).

A special wind tunnel model, machined from aluminum, was used in conjunction with the wire support apparatus (Figure 5). This model allowed four tungsten wires to be threaded through it and held securely by a set screw.

The eight tungsten wire ends were connected with turnbuckles to a rigid framework that surrounded the wind tunnel jet. The framework was in turn mounted on and supported by the diffuser. By adjusting the turnbuckles, the model could be positioned on the nozzle axis at zero angle of attack. Both 0.003 and 0.005 inch diameter wires were used successfully however, 0.003 inch wire proved to break too frequently for efficient tunnel operation.

2.4 Magnetic Model Suspension System

Conventional means of wind tunnel model support, such as a sting or wires, inevitably cause some degree of flow field interference. This represents an especially serious problem to the study of supersonic wakes of three-dimensional bodies. Magnetic model suspension makes possible interference free measurements and offers an opportunity to obtain data which might otherwise be unavailable.

The M.I.T. Aerophysics Laboratory operates a five degree of freedom magnetic model suspension system in conjunction with its hypersonic wind tunnel (7). It consists of five feedback control loops which control the currents in five electromagnets. This allows the operator to adjust and maintain model position in horizontal, vertical and axial translation and pitch and yaw rotation.

A schematic diagram of the magnet configuration is presented in Figure 6. A functional block diagram of the slip and yaw control loops appears in Figure 7 and a circuit diagram appears in Figure 8. The slip and yaw loops are typical of the others.

2.5 Instrumentation

2.5.1 Pitot Pressure - The primary instrument utilized in this investigation was the pitot probe. This instrument is the simplest and most reliable device available. Furthermore, the data it provides is less subject to interpretive errors than that provided by other devices.

Probes were constructed of stainless steel Vita Needle tubing mounted on brass double wedge stems (Figure 9). Dimensions of the probe tip are 0.025 inches O.D. and 0.0125 I.D.

The pitot probe was supported by a motor driven probe drive capable of being translated in three orthogonal directions: vertical, horizontal and axial. Potentiometers provided a signal proportional to probe position allowing pressure vs. position to be recorded continuously on an HP 7044A x-y plotter.

The signal proportional to pressure was provided by a Statham PA208TC-5-350 pressure transducer (Figure 9). In this experiment, the pitot probe served in the additional role of model support during wind tunnel start-up. Since the magnetic suspension system was unable to withstand the

large transient loads on the pyramid model during a tunnel start, models were slipped over the pitot probe in order to restrain their movement (Figure 10). After the tunnel reached steady state conditions, the probe was withdrawn by moving the probe drive downstream.

2.5.2 Aerodynamic Drag - Since the magnetic model suspension system compensates for all aerodynamic forces with corresponding and opposite magnetic forces, it is possible, in principle, to calculate all the aerodynamic loads on a wind tunnel model by measuring the currents in the system's magnets (8). In practice, interactions between the five degrees of freedom make this very difficult. However, in the special case of zero angle of attack, the situation is much simpler and the current in the drag magnet can be calibrated with reasonable accuracy for the measurement of aerodynamic drag (5). This is accomplished by pulling axially on a model with weights connected to the model by a thread strung over a pulley as illustrated in Figure 11.

A shunt in series with the drag magnet provides a signal proportional to drag current. This signal is fed to both a panel meter and a digital voltmeter with printer.

III. Data Reduction

3.1 Test Matrix

3.1.1 Pitot Pressure Profiles - Horizontal, vertical and axial traverses of the near wake in the region

from the base to three diameters aft have been taken. Measurements were made at two nominal stagnation pressures, 40.0 psia and 90.0 psia. The corresponding unit Reynolds numbers are 49,500 and 111,000 per inch. The nominal stagnation temperature and Mach number were constant throughout the tests at 470°F and 6.3, respectively.

With the model supported by 0.003 inch diameter wires, 17 traverses were made at P_o = 90.0 psia: 4 horizontal, 6 vertical and 7 axial. These are listed in Table 1.

With the model supported by 0.005 inch diameter wires, two identical sets of 12 traverses were made, one set at P_o = 40.0 psia and the other at 90.0 psia. Each set included 3 horizontal, 4 vertical and 5 axial traverses. In addition, at 40.0 psia two traverses were made which illustrate the effect removing one of the eight support wires has on the flow field interference level. These traverses are listed in Tables 2 and 3.

With the model supported by the magnetic model suspension system, 14 traverses were made at P_o = 40 psia: 5 horizontal, 6 vertical and 3 axial. These are listed in Table 4.

3.1.2 Base Pressure vs. Reynolds Number - Base pressure was measured by positioning the tip of the pitot probe close to the model's base so that it was within the

recirculation region. Although the flow direction is not even closely aligned with the probe, the error incurred is not serious because the region is virtually stagnant (2). Thus this measurement provides the static pressure at the base.

With the model supported by 0.005 inch diameter wire the pitot probe was held stationary at X/D = 0.058 diameters aft of the base and nearly on axis[1]. The free stream stagnation pressure was decreased in 10 psia increments from 90.0 psia to 30.0 psia and the base pressure was recorded at each point (Table 3).

With the model supported magnetically, the pitot probe was not positioned as close to the base as above in order to avoid the problem of interrupting the light beam used by the magnetic suspension system to measure the axial location of the model. Instead the probe was held stationary and on axis at X/D = 0.28, slightly downstream of the recirculation region. The free stream stagnation pressure was increased in 5 psia increments from 40.0 psia to 60.0 psia and the pressure was recorded at each point (Table 5).

---

[1]The probe was slightly off from the desired on-axis position: Y/D = -0.0056 and Z/D = 0.010.

3.1.3 Drag Coefficient vs. Reynolds Number - During the run described immediately above in which the "base pressure" of a magnetically suspended model was measured, the aerodynamic drag was measured simultaneously (Table 6). Aerodynamic drag was also measured on a previous occasion and over a wider range of Reynolds number. In this case the stagnation pressure was varied in 2 psia increments from 30.0 psia to 100 psia (Table 7).

3.2 Accuracy of Model Position and Angle of Attack

There are several factors which combine to produce the uncertainty with which the position of the model with respect to the pitot probe is known. First, there is the uncertainty in the position of the probe. And second, there is the uncertainty in the position of the model, which depends on the method of model support.

Mechanical counters on the probe drive allow the probe position to be monitored to within ± 0.001 inches on all three axes. The correspondence of a particular counter reading to some reference point is calibrated to within ± 0.001 inches on all three axes. The reference point depends on the method of model support.

With wire support, the model is installed in the tunnel first and is then itself used as the reference point for calibrating the probe drive counters. Consequently, the total uncertainty in the position of the probe with respect

to the model is ± 0.002 inches on all axes. The tolerance on angle of attack is ± 0.2 degrees for both pitch and yaw. The tolerance on roll is ± 0.9 degrees.

With magnetic support, both the probe position and the model position are referenced to the wind tunnel nozzle. Uncertainty in the probe position is ± 0.002 inches on all axes. Ideally, uncertainty in model position is of the order of ± 0.005 inches after the operator sets the position using the "absolute position" optics. There is an additional drift of ± 0.002 inches during the 10 minutes it takes to traverse the wake. The total positioning error of the model with respect to the probe is ± 0.009 inches.

Unfortunately, the optical system used to "absolute position" magnetically suspended models at their nominal location with respect to the nozzle could not be used (except in the axial direction) for a variety of reasons, during the collection of most of the data. Consequently, it was necessary to infer the position of the model with respect to the probe after completing the experiment using prominent features of the pitot pressure profiles such as the bow shock. A statistical analysis of the scatter in the data reveals the standard deviation in horizontal and vertical position to be 0.024 inches. The errors in pitch and yaw are estimated to be ± 1.4 degrees and the error in roll is estimated at ± 2.5 degrees.

3.3 Accuracy of Pitot Pressure Measurements

The uncertainty associated with the pitot pressure measurements depends mostly on the accuracy with which the transducer is calibrated and the precision with which the transducer output is recorded. The Statham transducer was carefully calibrated with an MKS Baratron Type 77 pressure meter to within 0.1 percent of reading ± 0.01 mm Hg. The calibration curve is presented in Figure 12. Transducer output was recorded on a Hewlett Packard 7044A X-Y plotter with a typical resolution of ± 0.1 mm Hg (± 0.02 mm Hg on axial traverses).

For a typical pitot profile, pressures ranged from a maximum of 100 mm Hg at the bow shock to a minimum of 1 mm Hg in the viscous core. The corresponding errors in measured pitot pressure are 0.2 percent at the bow shock and 10 percent in the viscous core (3% on axial traverses).

When measuring base pressure, transducer output was recorded with a digital voltmeter to within 0.2 percent. Thus, errors in base pressure attributable to the transducer are of the order of 1 percent.

There are other factors which can lead to non-ideal behavior of a pitot probe (2). These would include misalignment of the probe to the flow direction and viscous effects. It has been estimated that the error due to these effects is at most a few percent, except in the recirculation region. No corrections for these effects have been applied to the data in this report.

3.4 Drag Coefficient

The error associated with the aerodynamic drag measurements depends on the accuracy with which the drag current is calibrated and the accuracy with which the model is positioned at zero angle of attack.

Errors in calibration have been estimated to be within 7 percent. The calibration curve for drag magnet current as a function of drag force at zero angle of attack is presented in Figure 13.

At the time drag was measured over the stagnation pressure range from 30 to 100 psia, the model was not absolute positioned. Thus the tolerance on angle of attack was approximately ± 1.4 degrees (Section 3.2). The resulting error in drag measurements has been estimated at 2 percent.

At the time drag was measured over the stagnation pressure range from 40 to 60 psia (Run 63), the model was in absolute position. Thus the tolerance on angle of attack was better, on the order of ± 0.5 degrees, and the error is estimated at 1 percent.

The reference area used in the calculation of the drag coefficient was the base area (0.127 square inches). The Reynolds number calculation was based on $M_\infty = 6.32$ and $T_o = 470^oF$ with air treated as a perfect gas obeying Sutherland's formula for viscosity (9).

IV. Experimental Results and Discussion

4.1 Wire-Supported Pyramid

4.1.1 Support Interference

Pitot pressure measurements in the wakes of wire-supported models indicated a very high level of flow field interference due to the support wires (10). In fact, it was found that (except directly behind the model's fins) the wire disturbance was the most prominent feature of the flow field, obscurring even the bow shock. This clearly demonstrates the value of magnetic model suspension in wind tunnel work.

Despite the high level of interference, this data has proved to be useful, particularly with regard to measurements of base pressure and the extent of the re-circulation region. In order to avoid the problem of interrupting any of the magnetic suspension system's light beams with the pitot probe, the probe was kept at least 0.300 inches aft of the model's base. Thus, wire supported models afforded us our only opportunity to make measurements within the recirculation region.

4.1.2 Recirculation Region

The recirculation region, since it is nearly stagnant, is a region of nearly constant pressure. In the vicinity of the stagnation point at the rear of the recirculation region, streamlines which have expanded around the corner at the model's base must be returned to the free stream direction and the fluid undergoes

a recompression. Consequently, the location of the rear stagnation point and the extent of the recirculation region can be associated with the point on an axial pressure profile where the pressure begins to increase rapidly above the level at the base.

Pitot pressure profiles along the model's axis were taken at 90 psia with 0.003 inch diameter support wires (Run 7b) and at both 40 and 90 psia with 0.005 inch diameter wires (Runs 14 and 26, respectively). These profiles appear in Figures 14, 15 and 16. They cover the region from X = 0.020 to X = 3.000 inches aft of the base[2].

The rear stagnation point is located at X = 0.15, X = 0.13 and X = 0.12 inches for Runs 7b, 14 and 26, respectively. The most natural length scale for the recirculation region is the internal rib span, S_i, of 0.168 inches[3]. Non-dimensionalizing the length of the recirculation region, ℓ_r, with this figure gives $\ell_r/S_i = 0.89$, $\ell_r/S_i = 0.77$ and $\ell_r/S_i = 0.71$ for Runs 7b, 14 and 26.

---

[2] A cartesion coordinate system with origin at the center of the model's base is used. The axial coordinate is X, horizontal coordinate is Y and vertical coordinate is Z.

[3] Remember that the leading edge is not a streamline (attached shock). Thus there is no streamline along the leading edge which separates at the base and encloses the recirculation region.

These results are in excellent agreement with those presented by Martelluci, et al. (11), which showed that for $M_\infty \geq 5$, the rear stagnation points for cones, wedges and cylinders were all located around 0.8 base diameters downstream of the base.

The recirculation region is also visible in some of the horizontal and vertical traverses taken at X = 0.119 inches aft of the base. For example, Run 5b, which is a horizontal traverse at Z = 0 and Run 5, which is a vertical traverse at Y = 0.110 inches (Figures 17 and 18).

The point to notice in both of these figures is the pressure minimum at the centerline surrounded on either side by a slight increase in pressure and then a stretch where the pressure gradient is milder. A possible interpretation of this is a recirculation region surrounded on either side by a lip shock of virtually zero strength.

4.1.3 Constant Pressure Maps - Axial traverses, in either the vertical or horizontal plane of symmetry in which the model's fins lie (Y=0 or Z=0), were made at several spanwise locations and the results combined to form curves of constant pitot pressure. The results are presented for P_o = 90 psia and 0.003 inch diameter wires in Figure 19, P_o = 40 psia and 0.005 inch diameter wire in Figure 20 and P_o = 90 psia and 0.005 inch diameter wire in Figure 21.

The results of Blankson's study of the 7^{o} cone (2) are presented in Figure 22 for comparison. The most significant difference between them is the absence of a wake shock in the reentrant pyramid wake.

4.1.4 Base Pressure vs. Reynolds Number - Base pressures measured with the model supported by 0.005 inch diameter wire (Run 38) are plotted as a function of Reynolds number along with the free flight correlations of Cassanto, et al. (12) in Figure 23. The results of McLaughlin (1) and Blankson (2) also appear in this figure.

The base pressures measured on the wire-supported reentrant pyramid are higher by about a factor of three than the data for sharp cones. This is almost certainly the result of interference from the support wires in light of the fact that Blankson (2) found a similar increase in base pressure on 20% blunt cones. Further evidence of this appears in Section 4.2.5, where the base pressure measured on magnetically supported reentrant pyramids is discussed.

4.2 Magnetically-Supported Pyramid

4.2.1 Pitot Pressure Profiles - The interference free pitot pressure profiles taken in the wake of magnetically-suspended models are strikingly different from those taken in the wake of wire-supported models. With all the peaks and valleys due to support interference gone, the remaining features appearing in the profiles can be interpreted with

comparative ease. The bow shock, inviscid shock layer and viscous core are all easily discernable.

All of the interference free pitot profiles were manually digitized so that the axes could be scaled in a manner which allows several profiles to be presented together in one figure. Computation was performed at M.I.T.'s Multics computer facility and the resulting figures were drawn on a Calcomp plotter. Pitot pressure was non-dimensionalized with the free stream stagnation pressure and length was non-dimensionalized with the base diameter of 1.072 inches.

The four pitot profiles which appear in Figure 24. illustrate the axial development of the wake from the base to three diameters downstream. This is a side view of the wake in which all the profiles lie in the vertical plane at Y = 0.

Due to the large uncertainty in model position pointed out in Section 3.2, the positions of the profiles were adjusted to make them symmetrical about the centerline. This was accomplished by placing the midpoint of the bow shocks on the centerline or, when the bow shock was not present on both sides of the profile, by placing the mid-point of the full width at half maximum of the pressure in the viscous core on the centerline.

For comparison, the axial development of the sharp 7^{o} half angle cone wake studied by Blankson (2) at $M_{\infty} = 6.32$ and $Re_{\infty D} = 62,000$ is presented in Figure 25. This is the

same Mach number and nearly the same Reynolds number (Re_{∞_D} = 53,600) as for the reentrant pyramid.

The principal difference between the pyramid and cone wakes which can be seen in these figures is the absence from the pyramid wake of a wake shock of any appreciable strength.

Six pitot profiles taken in the plane X/D = 0.28 define the cross section of the pyramid wake just aft of the base. These profiles are presented in two rear views of the wake. Three horizontal profiles appear in Figure 26 and three vertical profiles in Figure 27.

The same methods as described for the profiles in the side view were used in these figures to position the profiles symmetrically about the pyramid's axis or behind one of the fins. This point will be discussed further in Section 4.2.2.

The profiles in Figures 26 and 27 are somewhat noisey due to oscillation of the model's position during the pitot pressure measurements. This consisted primarily of a rocking motion in the uncontrolled roll degree of freedom about a naturally stable position. The same profiles have been replotted in Figures 28 and 29 after being digitally low pass filtered to remove most of the noise.

Three axial pitot profiles covering the region from X/D = 0.28 to X/D = 2.85 are presented in a side view of the wake in Figure 30. The positions of these traverses in the Y-Z plane are shown schematically in a rear view drawn in the upper left corner of the figure.

Extrapolating the profile lying on the model's axis upstream to the base provides the best estimate of base pressure obtained in this study. The value obtained is $P_b/P_\infty = 0.58$ at $Re_{\infty \ell} = 9.85 \times 10^4$. This result is in good agreement with the free flight data of Cassanto (12), shown in Figure 23.

4.2.2 Shock Trace - The shock trace in the plane X/D = 0.28 has been estimated using the data presented in Figures 26 and 27. The pitot profiles were positioned so that the midpoint of the full width at half maximum of the viscous core was centered behind the model's fins. Then all the bow shock position data was combined on a single figure along with a least squares fit. We have taken advantage of the symmetry of the wake in order to increase the number of data points by reflecting the measured shock positions about the symmetry lines.

The results appear in Figure 31 and show that the shock trace is nearly circular. Taking advantage of the circular shape of the shock trace, we tried repositioning

the pitot profiles by placing the midpoint of the bow shocks on the line Y = 0 for horizontal traverses and on the line Z = 0 for vertical traverses. The data was then replotted with a new least squares fit in Figure 32. While the least squares fit for the shock trace is virtually identical to the previous one, the scatter in the data is significantly reduced, indicating that this method of positioning the profiles is superior.

4.2.3 Viscous Wake Edge - Blankson (2) has shown that the viscous wake edge location given by hot film recovery temperature profiles is strongly correlated to the point on pitot profiles where the pitot pressure begins to rapidly decrease toward the level at the center of the viscous wake.

Using this criterion the cross section of the viscous wake edge lying in the plane X/D = 0.28 has been determined. In Figure 33 the midpoint of the viscous core was used to position the data and in Figure 34 the circular shock trace assumption was used. Least square fits are shown in both cases and, again, the scatter in the data is less when the circular shock trace assumption is employed.

There is some possibility that the viscous wake edge location determined above is in error, since a decrease in pitot pressure can also be attributed to isentropic expansion. However, considering the large slope of the pitot profiles in the vicinity of the viscous wake edge, such errors will be minimal.

4.2.4 Near Wake Map - The results of the least squares fits to the shock trace and viscous wake edge in the plane X/D = 0.28 have been combined in Figure 35 to show the wake cross section divided into inviscid and viscous regions. The displacement of the bow shock from its "on design" location and the very thick viscous core are consistent with the degree of viscous interaction indicated by $\chi_\infty = M_\infty^3/\sqrt{Re_{\infty \ell}} = 0.80$.

A similar procedure has been followed, working with the data presented in Figure 24, to produce a side view of the bow shock and viscous wake edge in the plane Y = 0. The results are shown in the near wake map appearing in Figure 36.

A least squares fit to the bow shock shows that it is inclined 13.9° to the "free stream". Extrapolating upstream to the base indicates that the bow shock is attached to the leading edges.

Blankson's results for the sharp 7° cone are presented in Figure 37 for comparison. The bow shock on the cone is inclined 12° to the flow, close to that found on the pyramid, but the viscous core of the pyramid wake is much thicker.

4.2.5 Base Pressure vs. Reynolds Number - The base pressure data collected with a magnetically-suspended model has been included along with the data discussed in Section 4.1.4

in Figure 23. The present data shows good agreement with the free flight correlations of Cassanto (12), lending support to the conclusion that the higher base pressure found on the wire-supported pyramid was due to support interference.

4.2.6 Drag Coefficient vs. Reynolds Number - Results of the measurements of aerodynamic drag at zero angle of attack are presented in Figure 38. The rapid decrease in drag coefficient with increasing Reynolds number indicates significant changes in the wake are occurring.

V. Conclusions

5.1 Summary of Results

1. Wire model supports produce an unacceptably high level of flow field interference, as evidenced by wake profiles and a 310 percent increase in base pressure above that for magnetically-suspended models. This demonstrates the mandatory nature of magnetic model suspension in wind tunnel work with this shape.

2. The base pressure found for the magnetically-suspended reentrant pyramid and the location of the rear stagnation point found for the wire-supported reentrant pyramid are in good agreement with the findings of other researchers.

3. The bow shock trace was found to be nearly circular, a result which is consistent with the expected level of viscous interaction at the test Reynolds number.

4. No wake shock of appreciable strength was found in the reentrant pyramid wake.

5. A rapid decrease in drag coefficient with increase in Reynolds number was found over the range of the tests.

5.2 Comparison to Cones

The bow shock found for the reentrant pyramid (at $\chi_\infty = 0.80$) is nearly identical to that which would be present on a cone of semi-vertex angle equal to 9.5 degrees. However, there is a major difference in wake structure indicated by the absence of a wake shock from the reentrant pyramid wake.

5.3 Further Analysis

Analysis and interpretation of the data collected during this study is still under way and will be included in a forthcoming Ph.D. thesis. A copy of the thesis will be forwarded upon its completion.

5.4 Publications

A list of publications resulting from work performed under this contract follows:

1. Solomon, M, "A Study of the Lift-to-Drag Ratio Capability of Caret Wing Waveriders", S.M. Thesis, Dept of Aeronautics and Astronautics, MIT, Cambridge, Ma., May, 1977 (also, MIT Aerophysics Laboratory TR 200, March, 1978).

2. Solomon, M, "An Experimental Study of the Reentrant Pyramid Near Wake at Hypersonic Mach Number using Magnetic Model Suspension", Ph.D. Thesis, Dept. of Aeronautics and Astronautics, MIT, Cambridge, Ma., expected October, 1979.

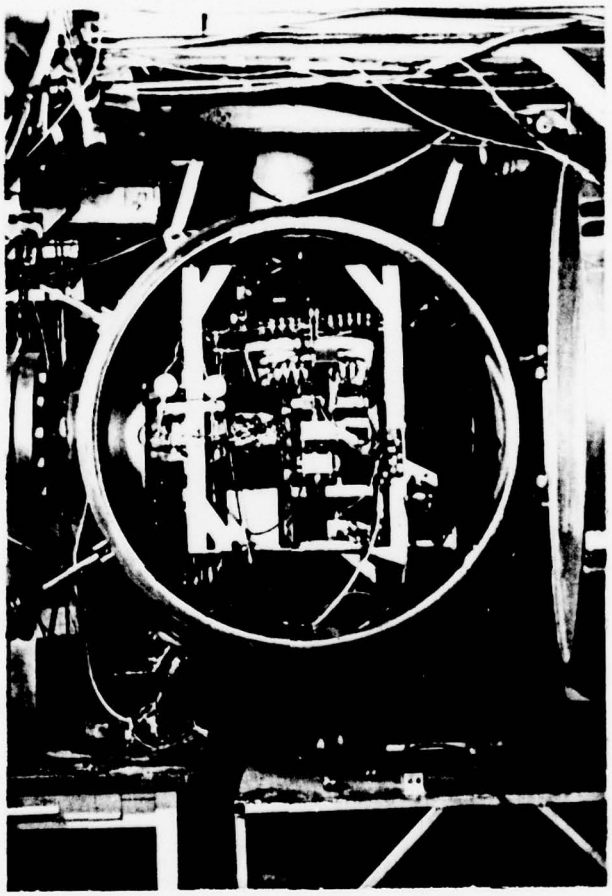

Figure 1. Hypersonic wind tunnel test section with magnetic model suspension system

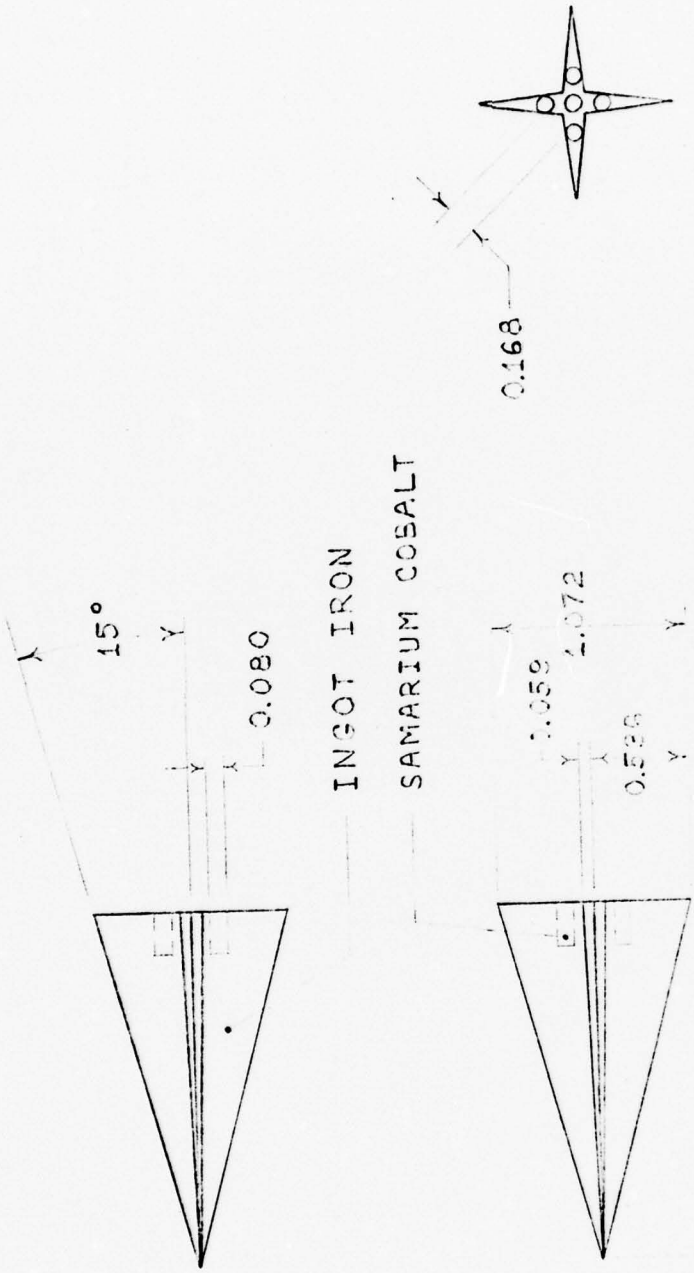

Figure 2. 15° reentrant pyramid

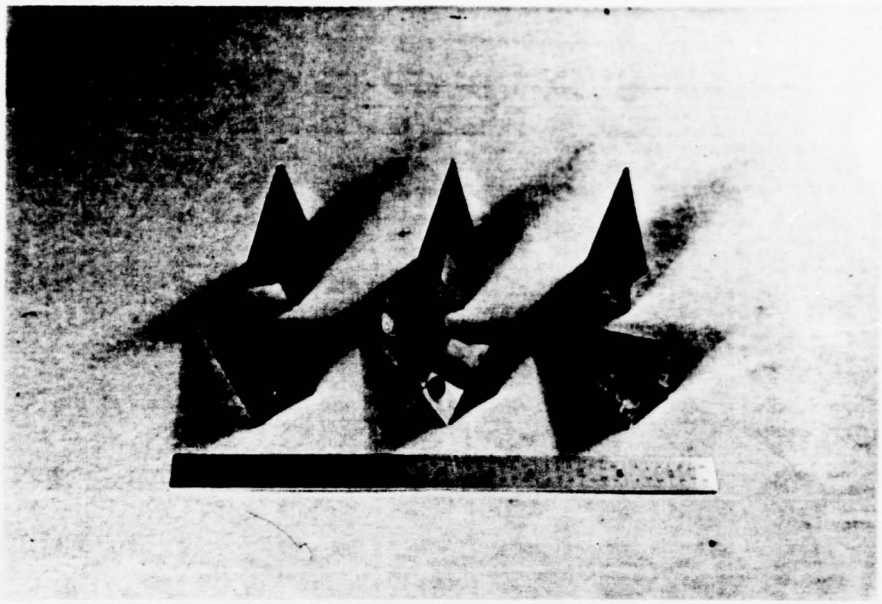

Figure 3. Reentrant pyramid wind tunnel models illustrating fin weighting schemes for roll control

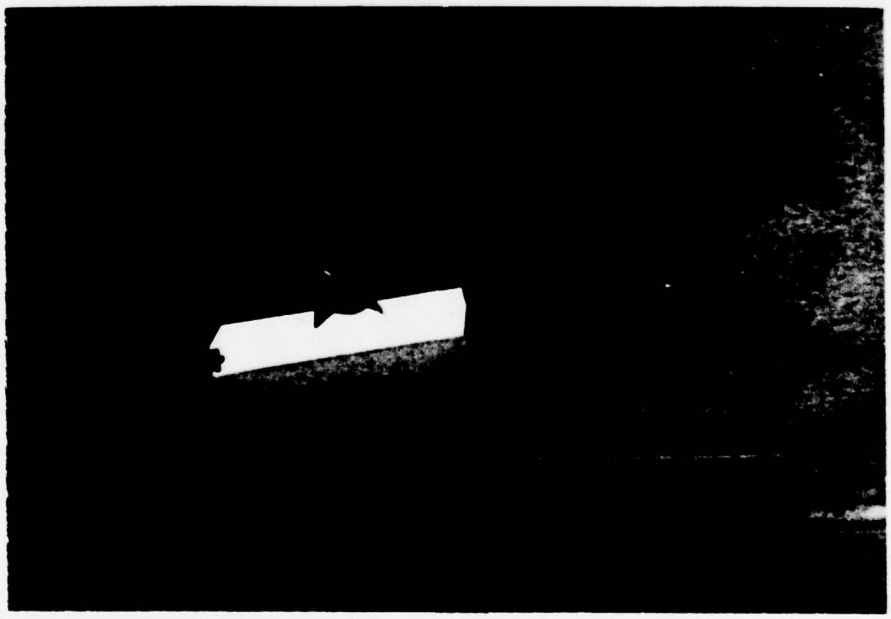

Figure 4. Reentrant pyramid wind tunnel model with samarium cobalt magnet in each fin

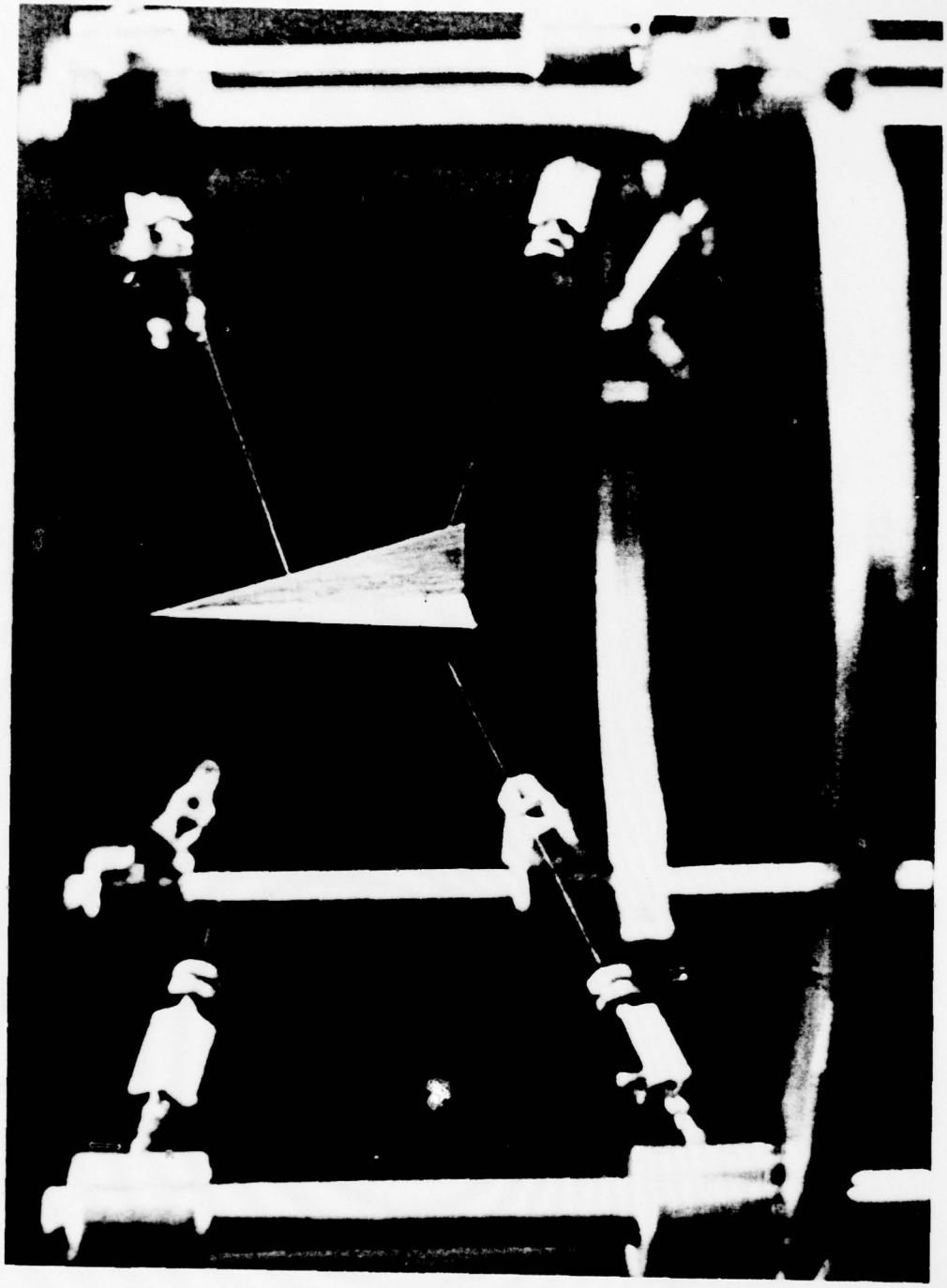

Figure 5. Reentrant pyramid wind tunnel model and wire suspension apparatus

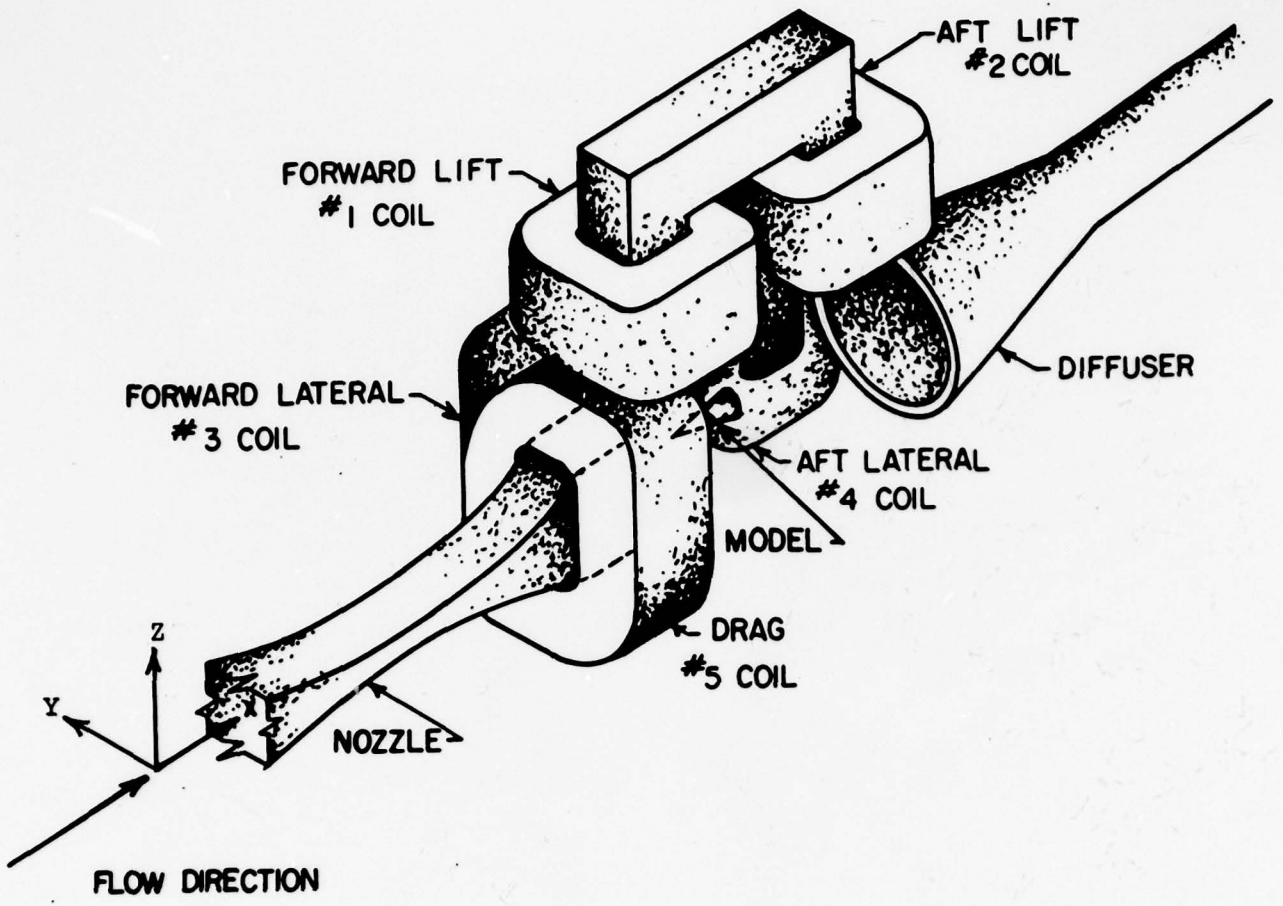

Figure 6. Magnet configuration of magnetic model suspension system

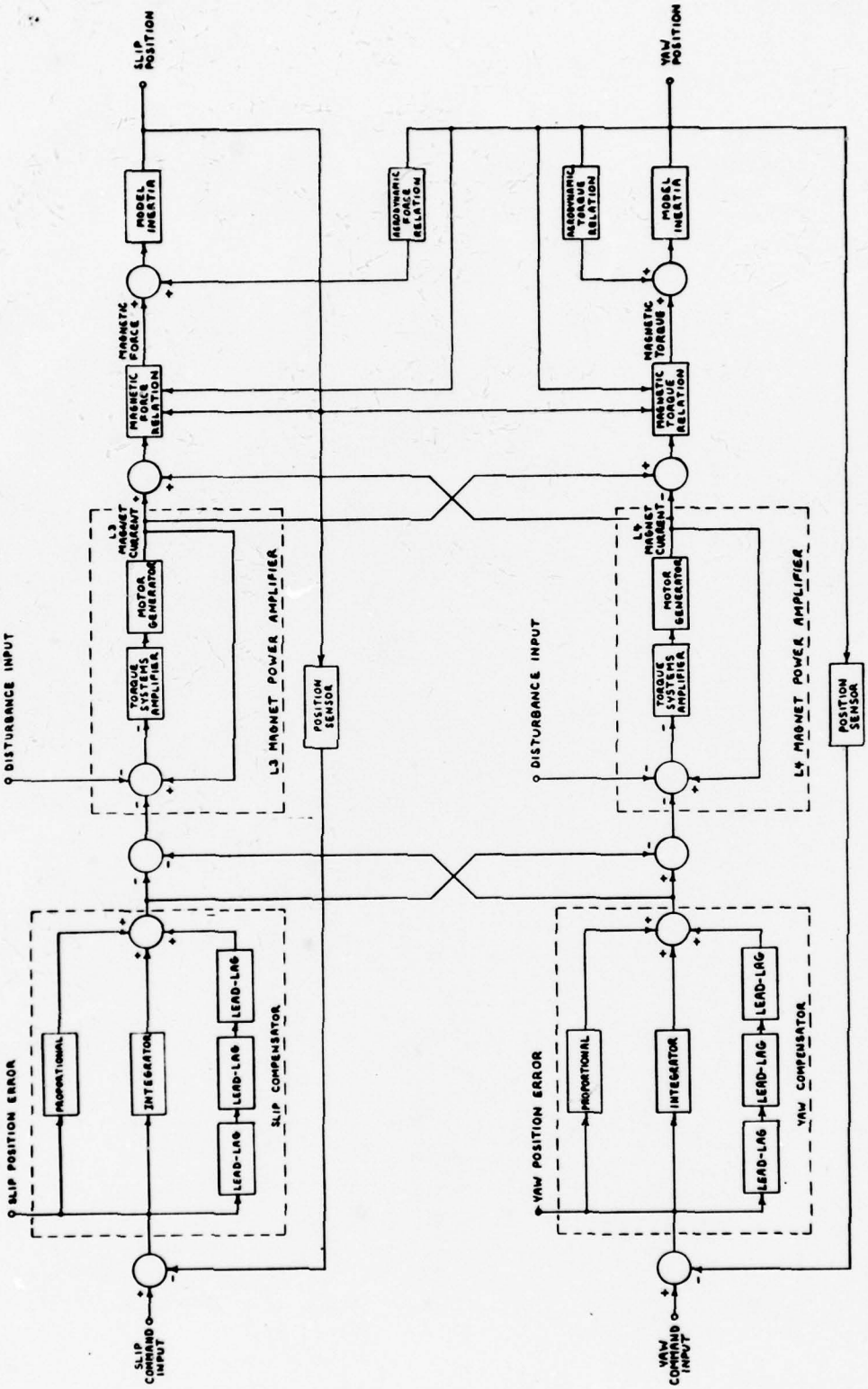

Figure 7. Slip and yaw control loops - functional block diagram

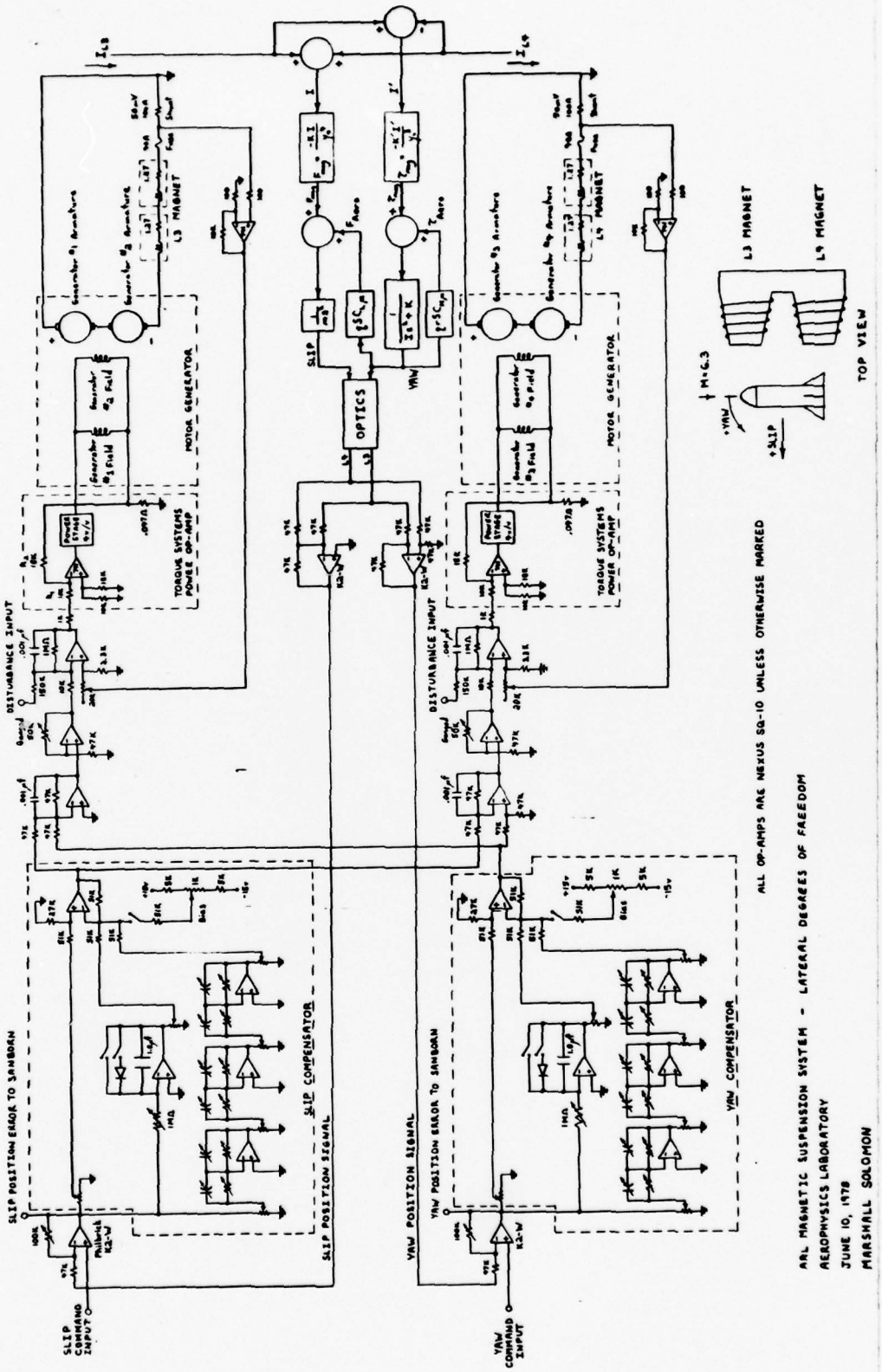

Figure 8. Slip and yaw control loops - circuit diagram

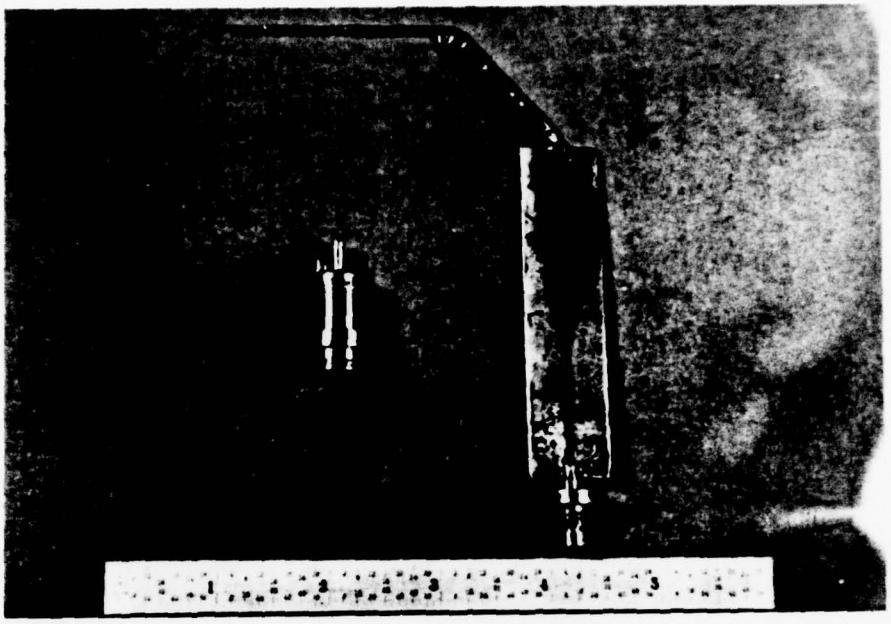

Figure 9. Pitot pressure probe and Statham pressure transducer

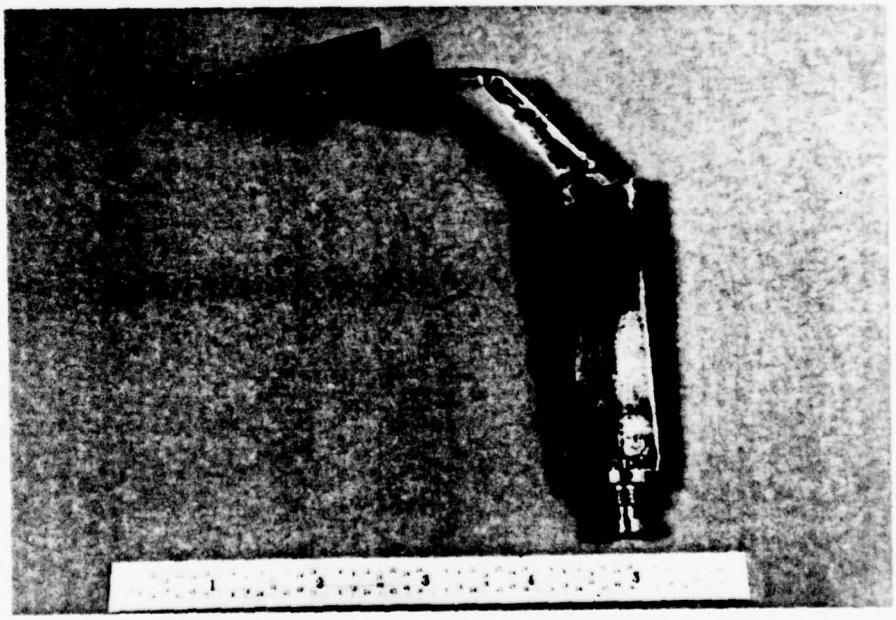

Figure 10. Reentrant pyramid wind tunnel model mounted on pitot pressure probe

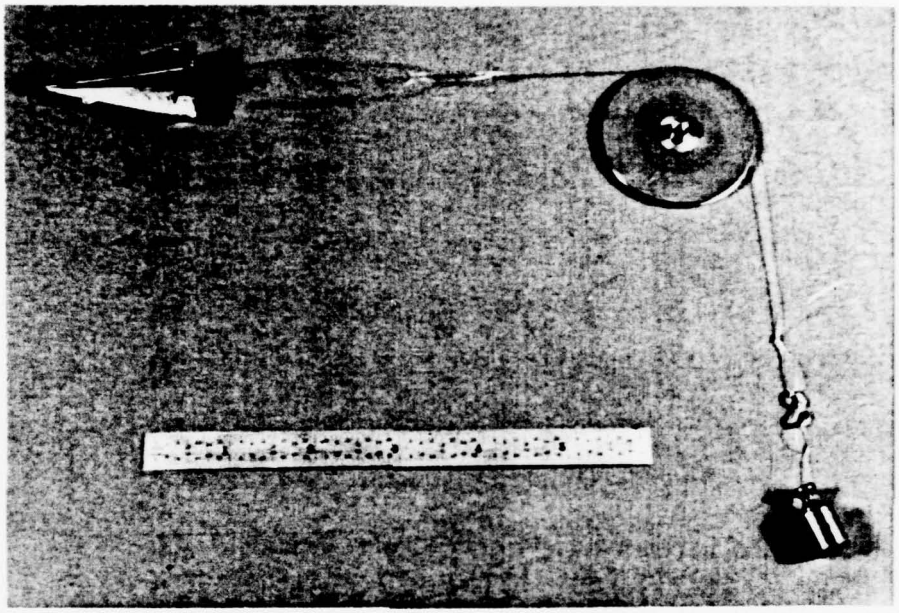

Figure 11. Calibration of current flowing through drag magnet for the measurement of aerodynamic drag

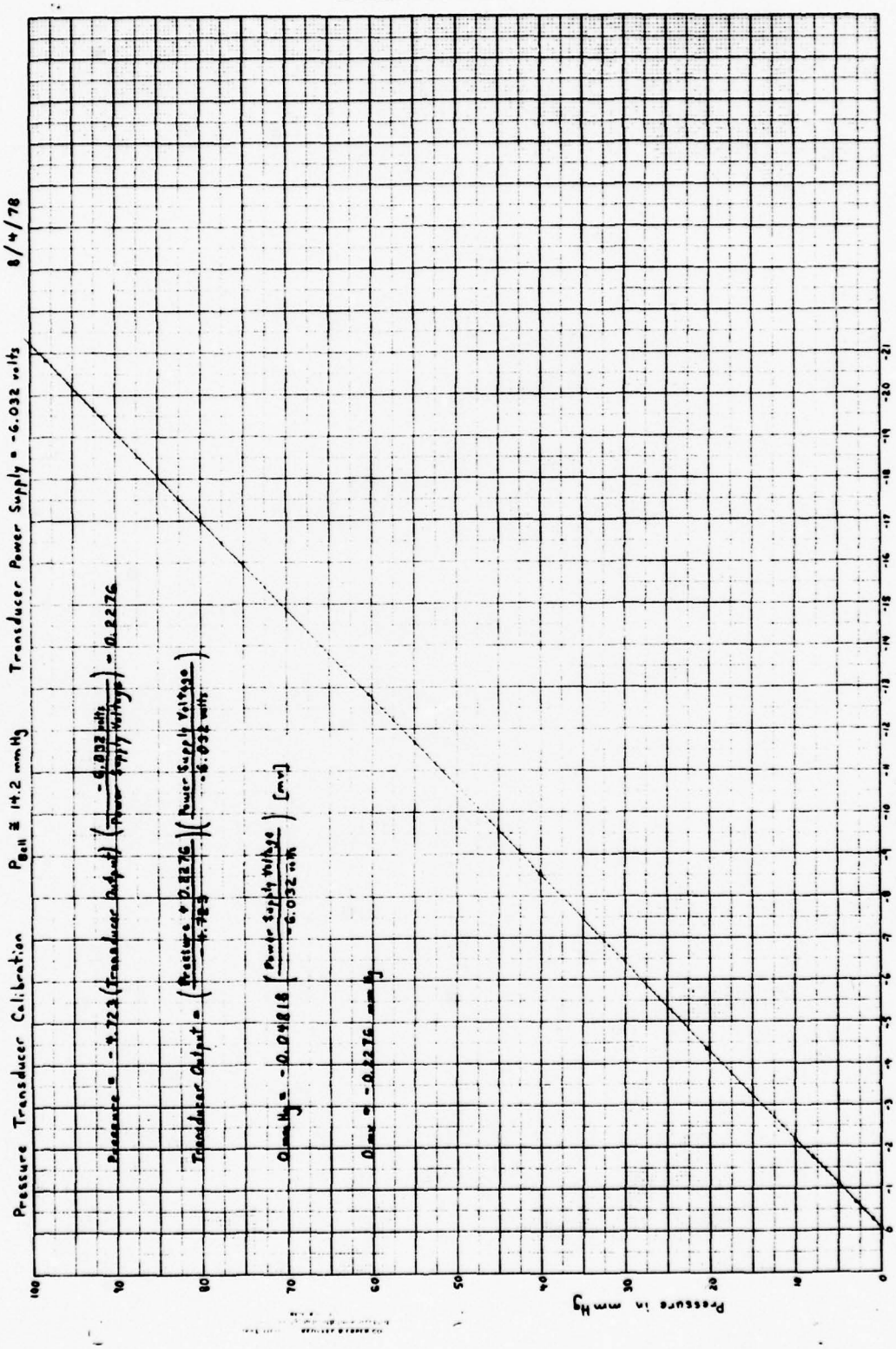

Figure 12. Calibration curve for Statham pressure transducer

Figure 13. Calibration curve of drag current vs. drag force at zero angle of attack

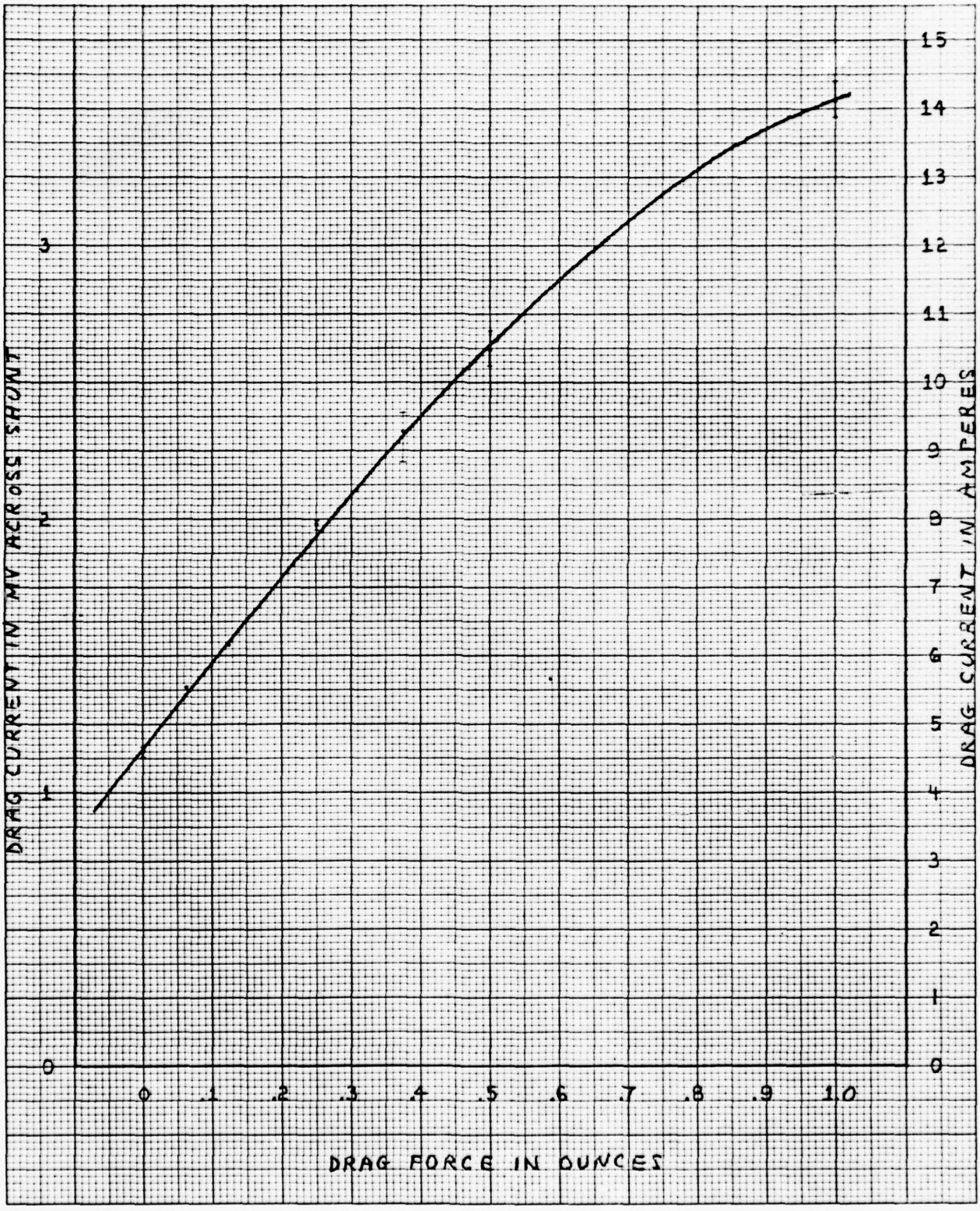

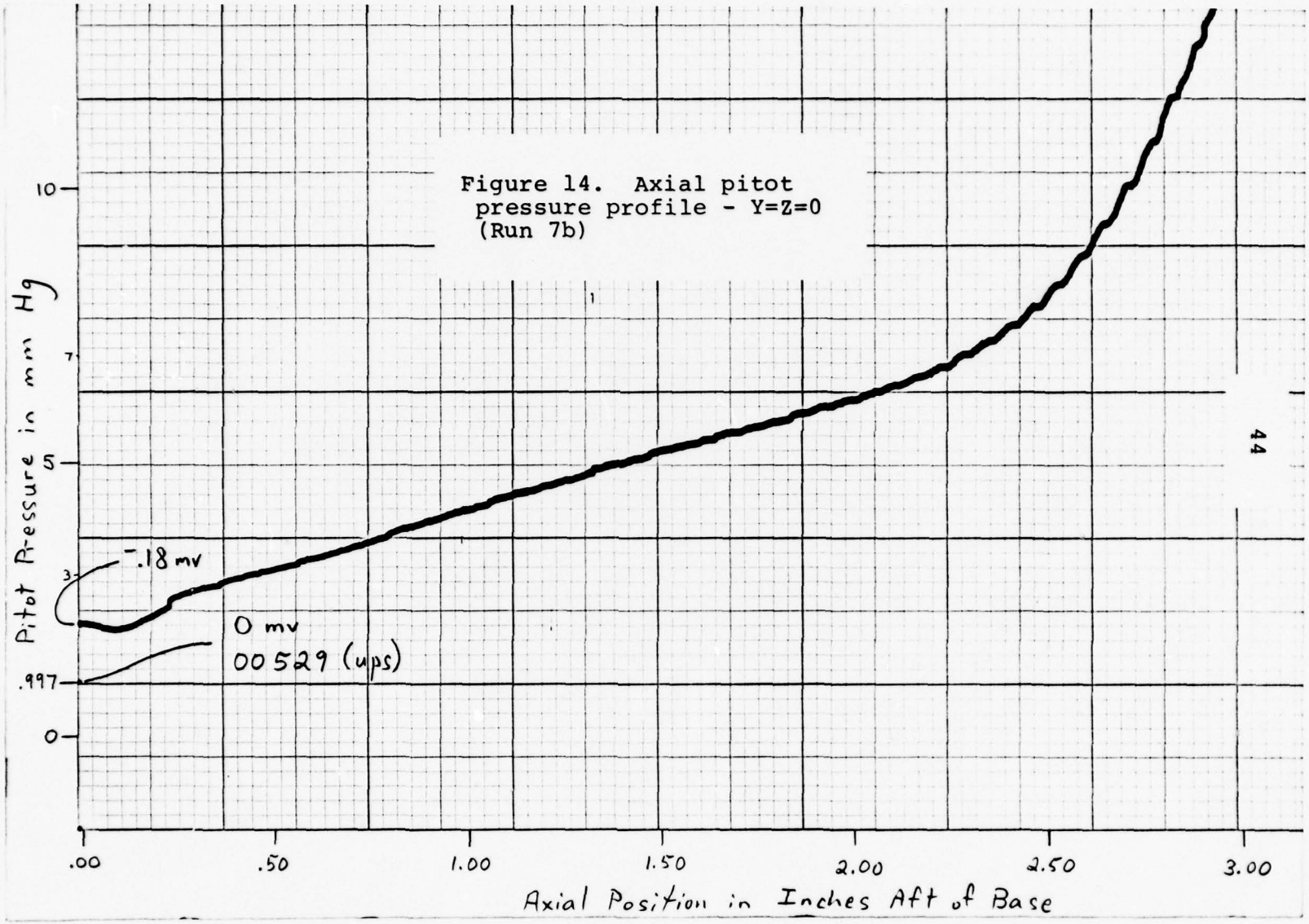

Figure 14. Axial pitot pressure profile - Y=Z=0 (Run 7b)

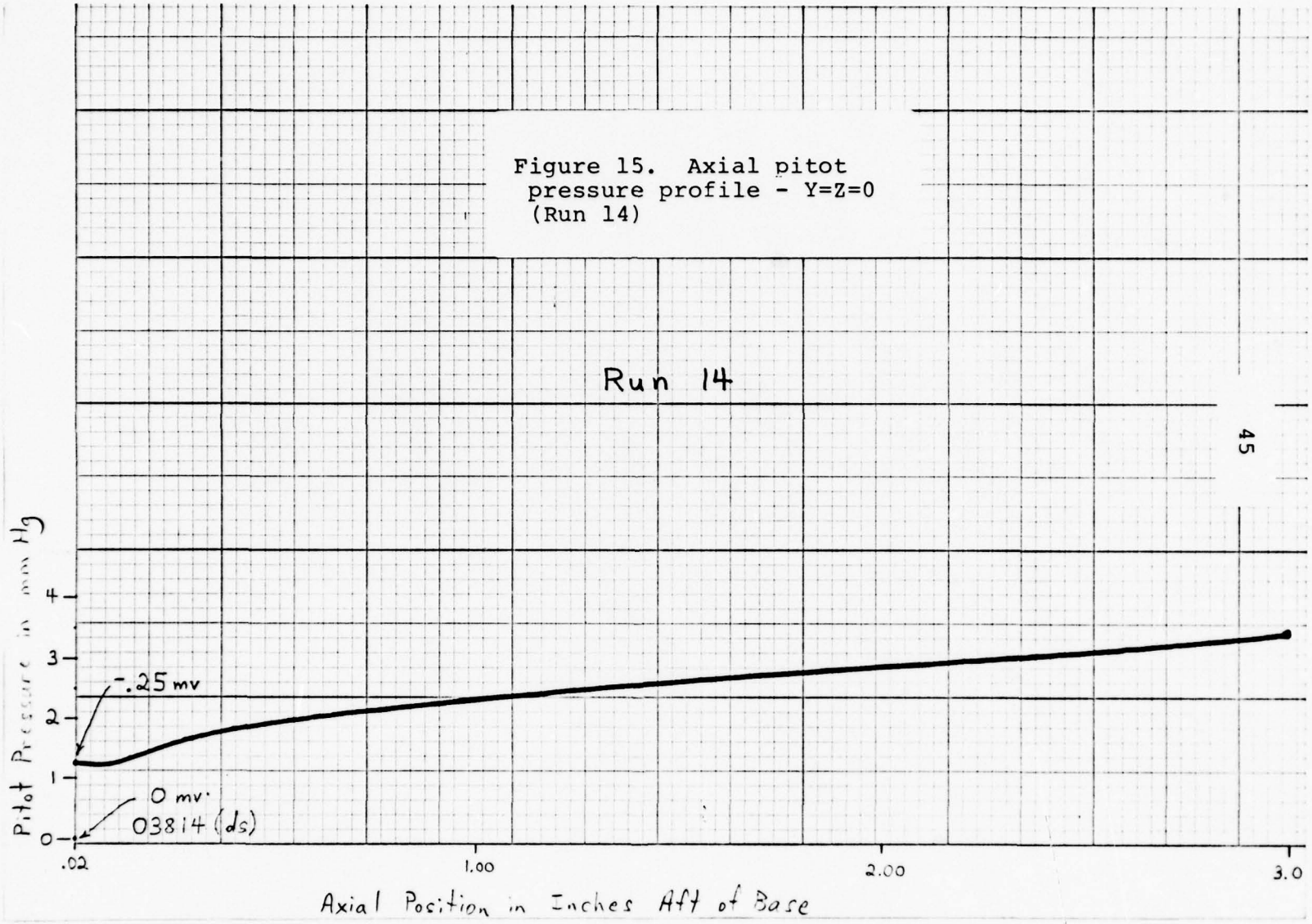

Figure 15. Axial pitot pressure profile - Y=Z=0 (Run 14)

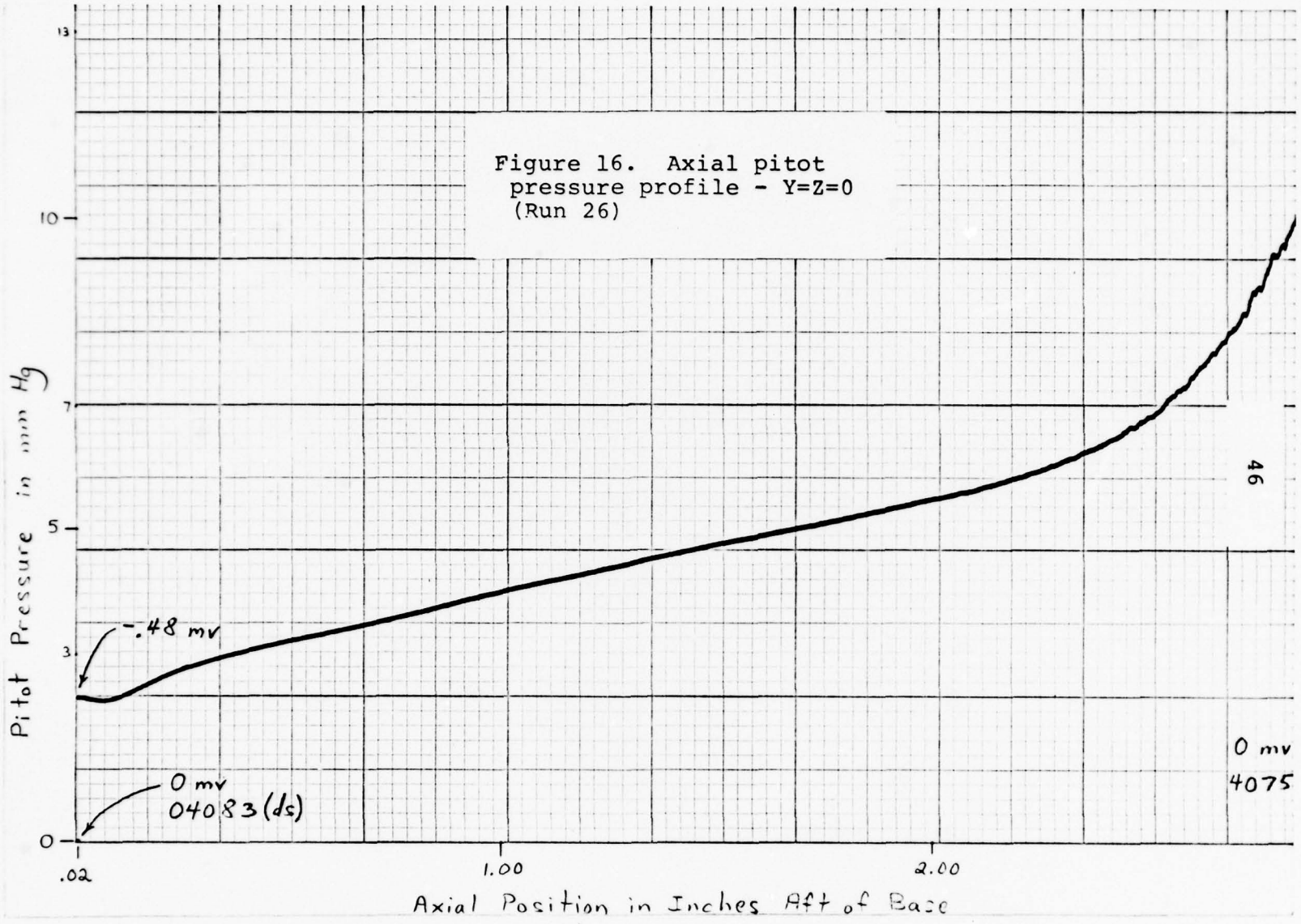

Figure 16. Axial pitot pressure profile - Y=Z=0 (Run 26)

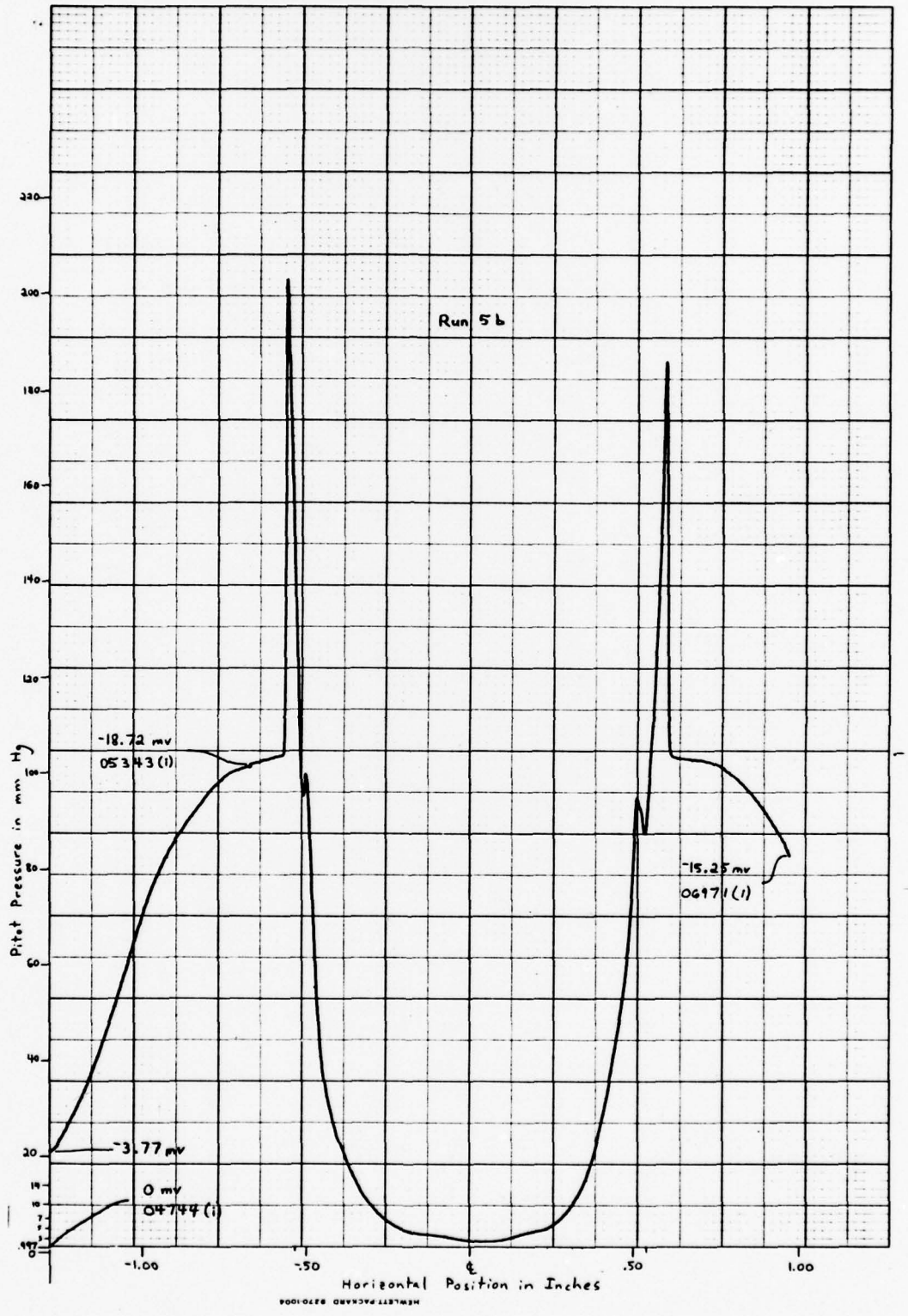

Figure 17. Horizontal pitot pressure profile - x = 0.119 inches and z = 0 (Run 5b)

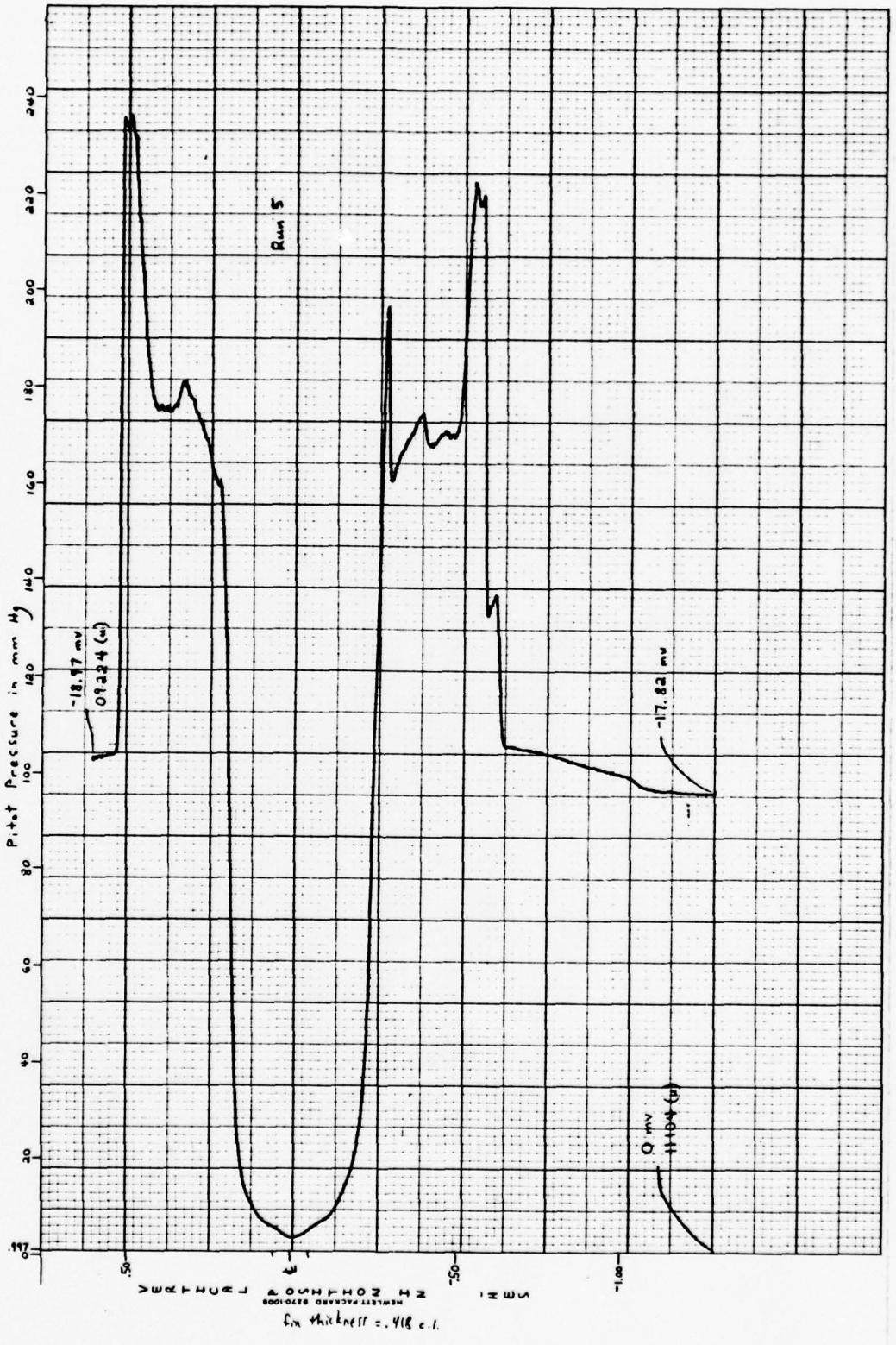

Figure 18. Vertical pitot pressure profile - x = 0.119 inches and y = 0.110 inches (Run 5)

Figure 19. Curves of constant pitot pressure - P_o = 90 psia - 0.003 inch diameter wire supported model

whole numbers in mm Hg
numbers in parenthesis are the ratio P_p/P_o

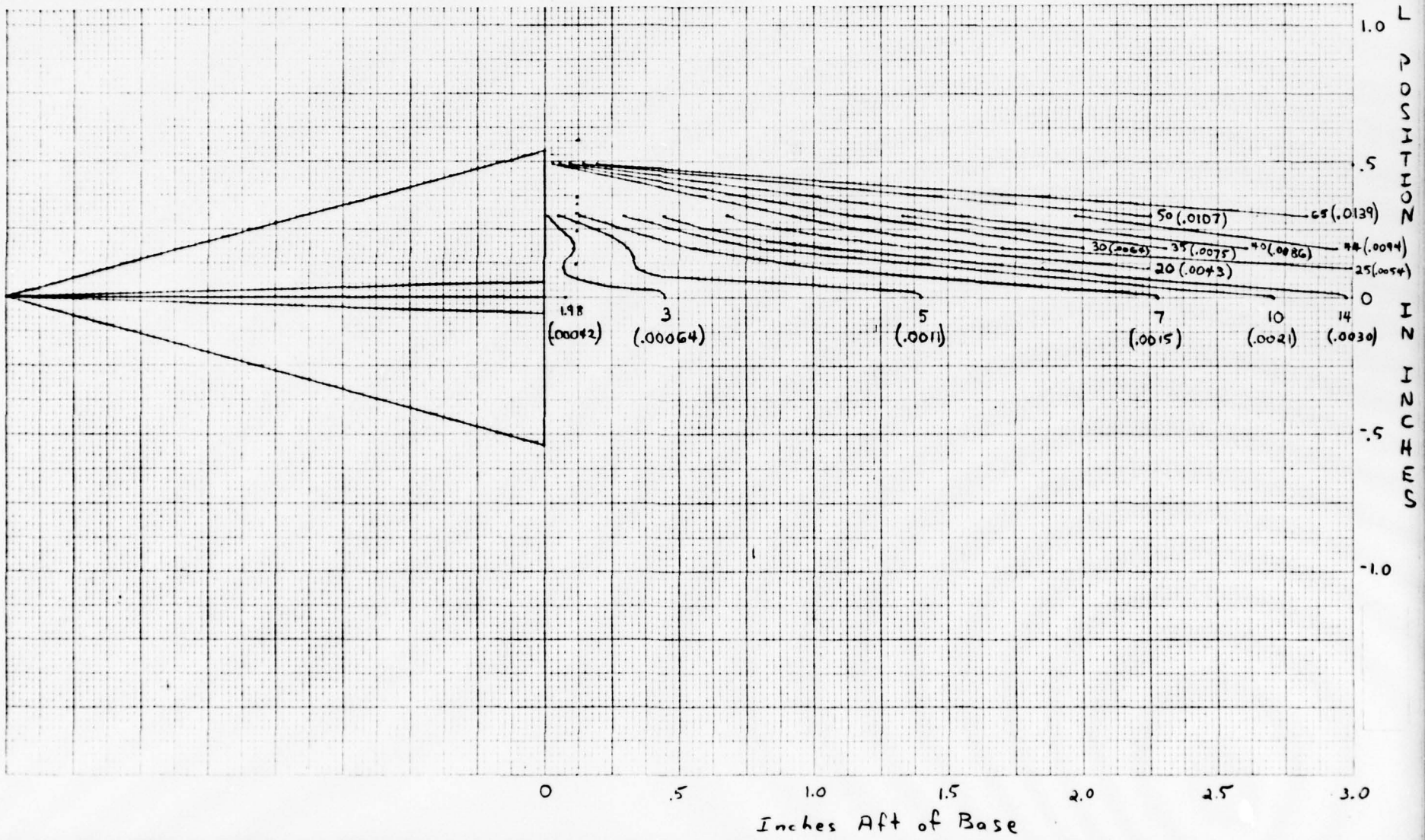

Figure 20. Curves of constant pitot pressure - P_o = 40 psia - 0.005 inch diameter wire supported model

whole numbers in mm Hg
numbers in parenthesis are the ratio P_p/P_o

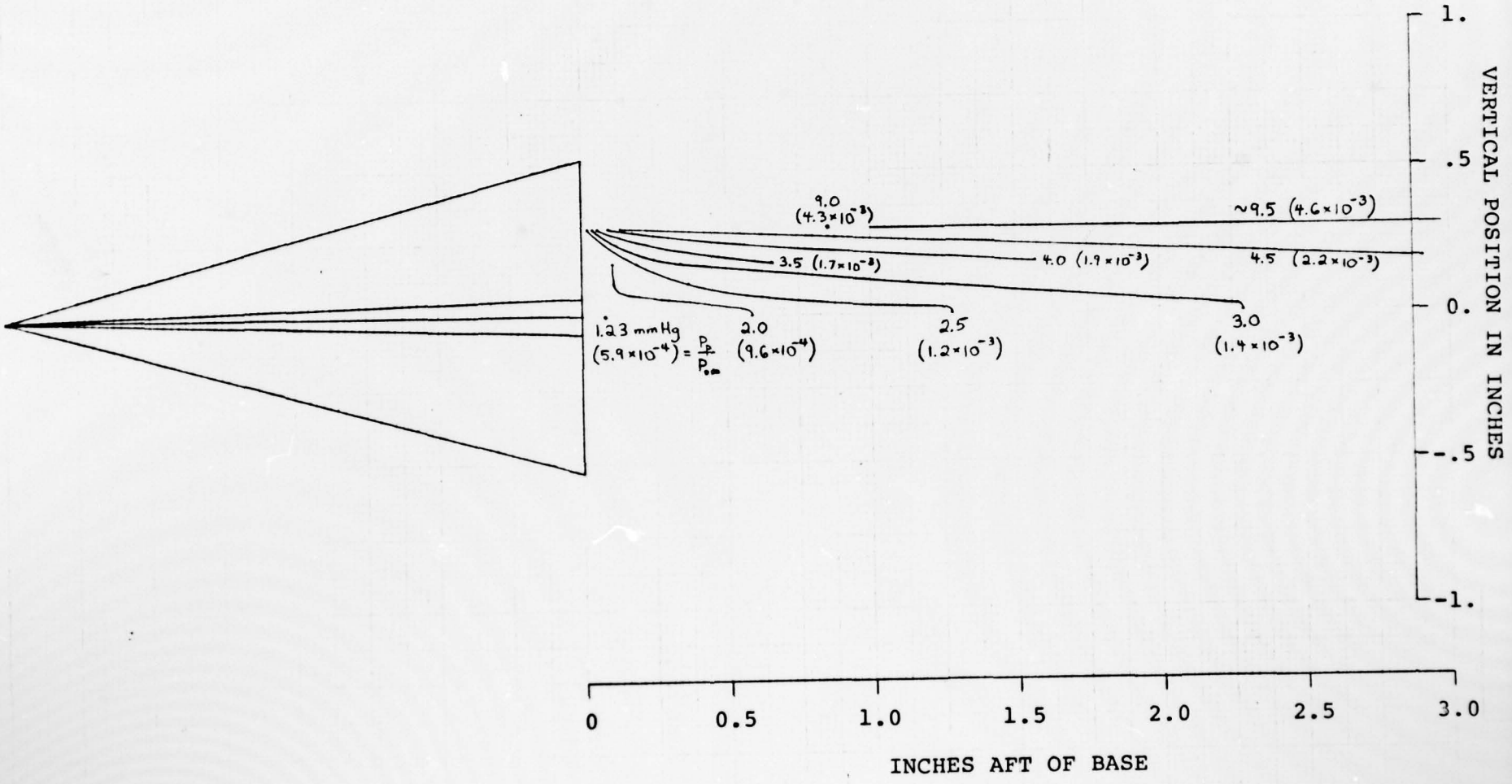

Figure 21. Curves of constant pitot pressure - P_o = 90 psia - 0.005 inch diameter wire supported model

whole numbers in mm Hg
numbers in parenthesis are the ratio P_p/P_o

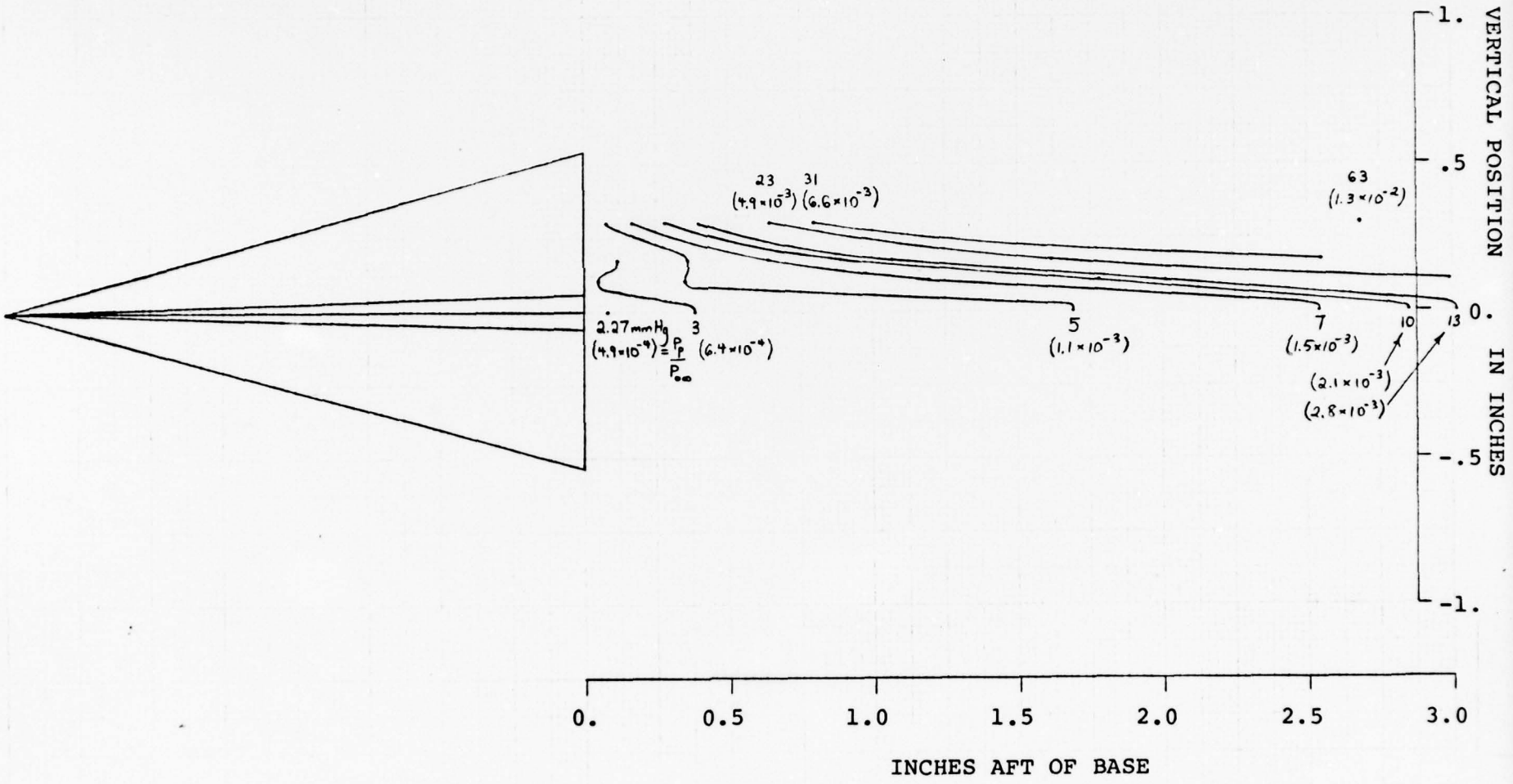

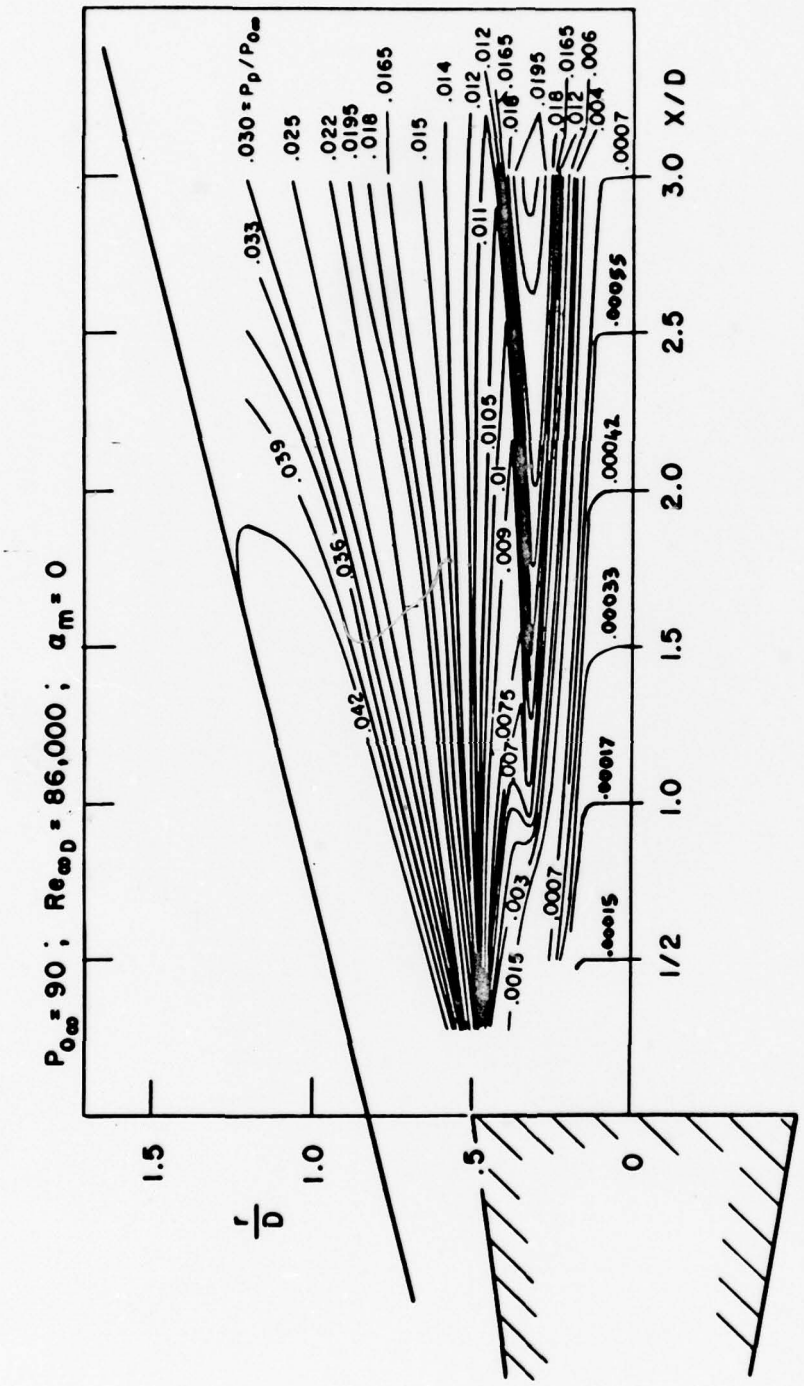

FIG. 22. CURVES OF CONSTANT PITOT PRESSURE - 7° half angle sharp cone

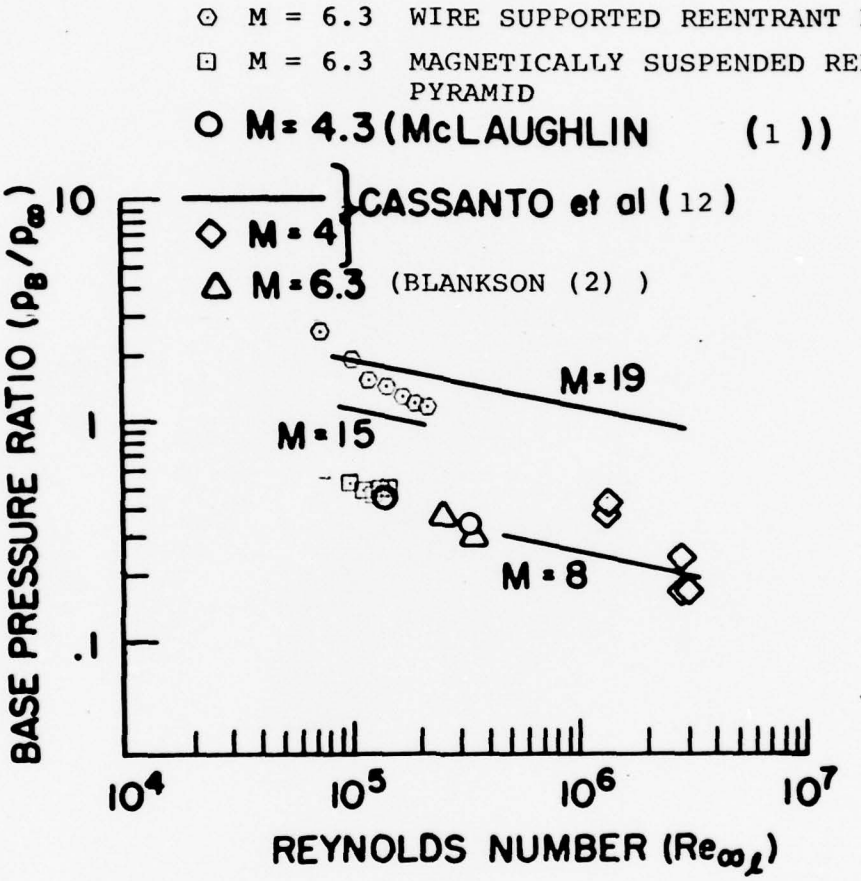

Figure 23. Correlation of base pressure vs. Reynolds number

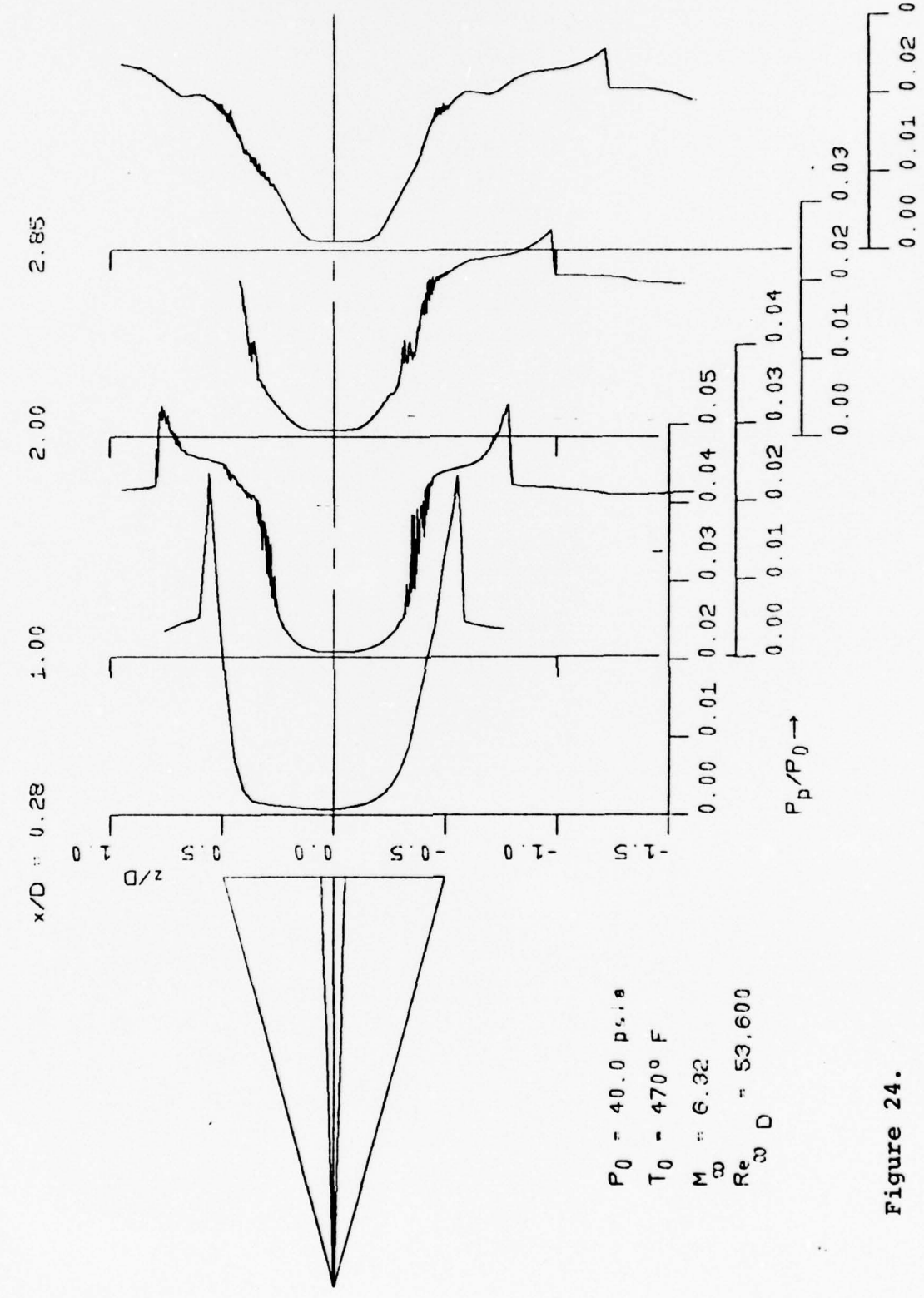

Figure 24.

PITOT PRESSURE PROFILES. 15 DEGREE REENTRANT PYRAMID.

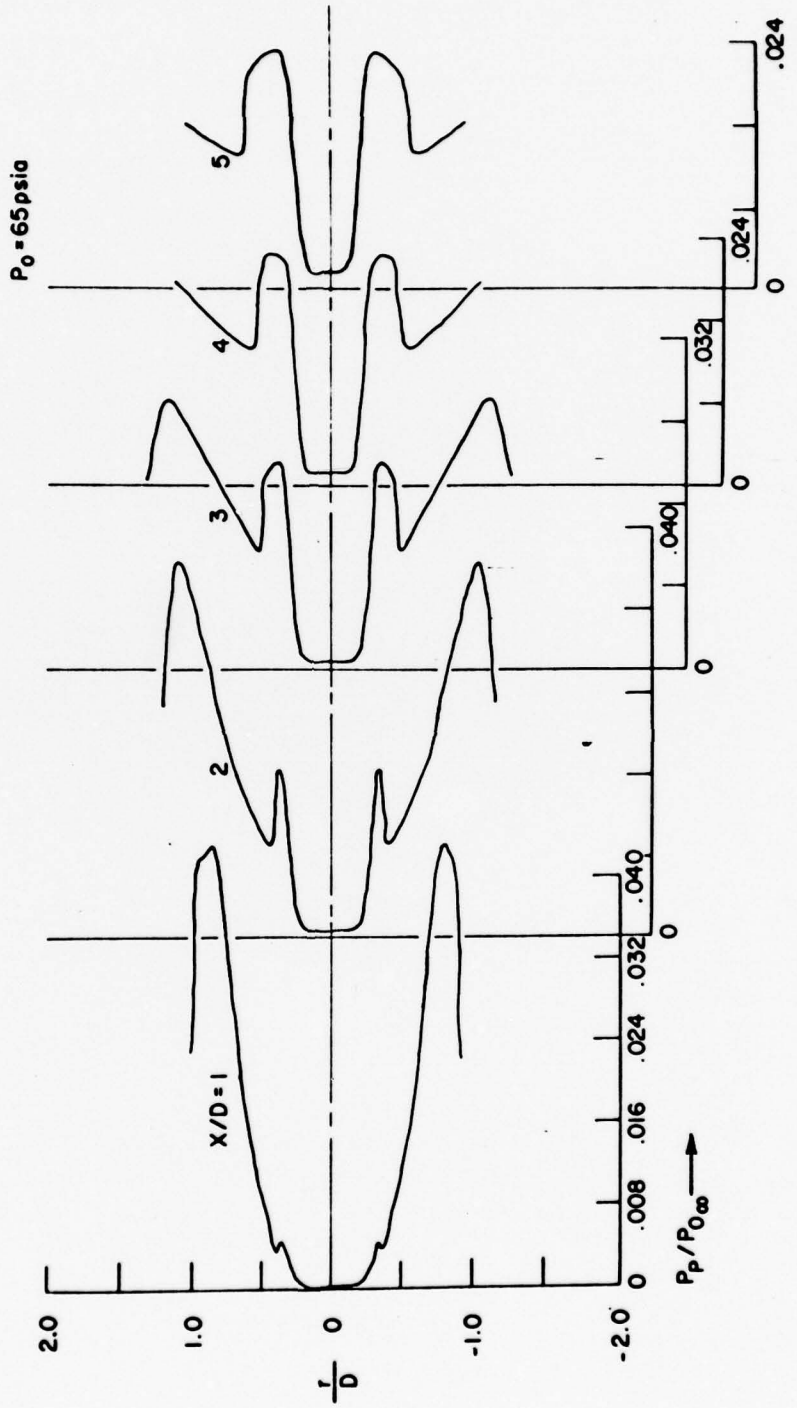

Figure 25. Pitot pressure profiles - 7° sharp cone

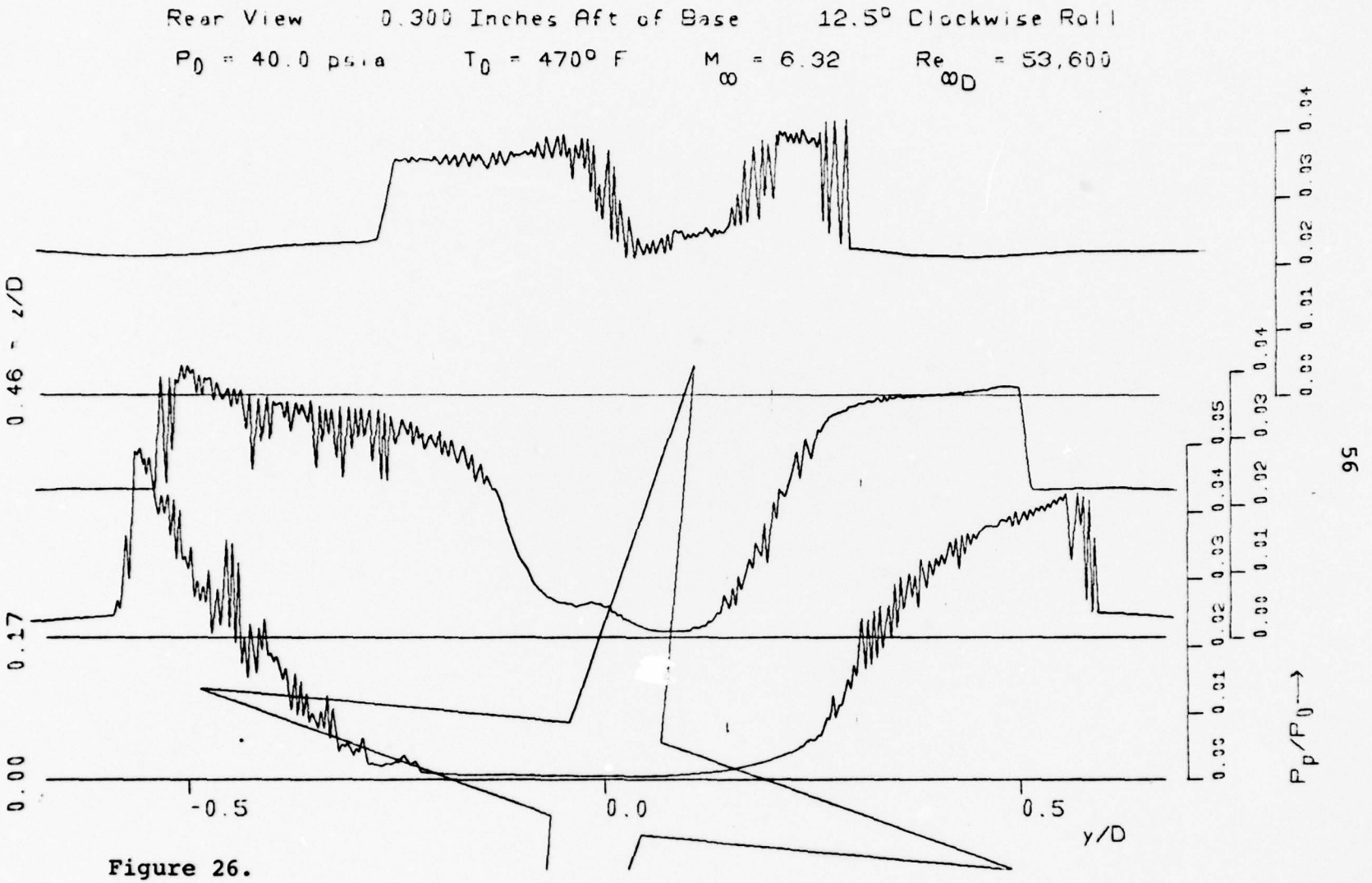

Figure 26.

PITOT PRESSURE PROFILES. 15 DEGREE REENTRANT PYRAMID.

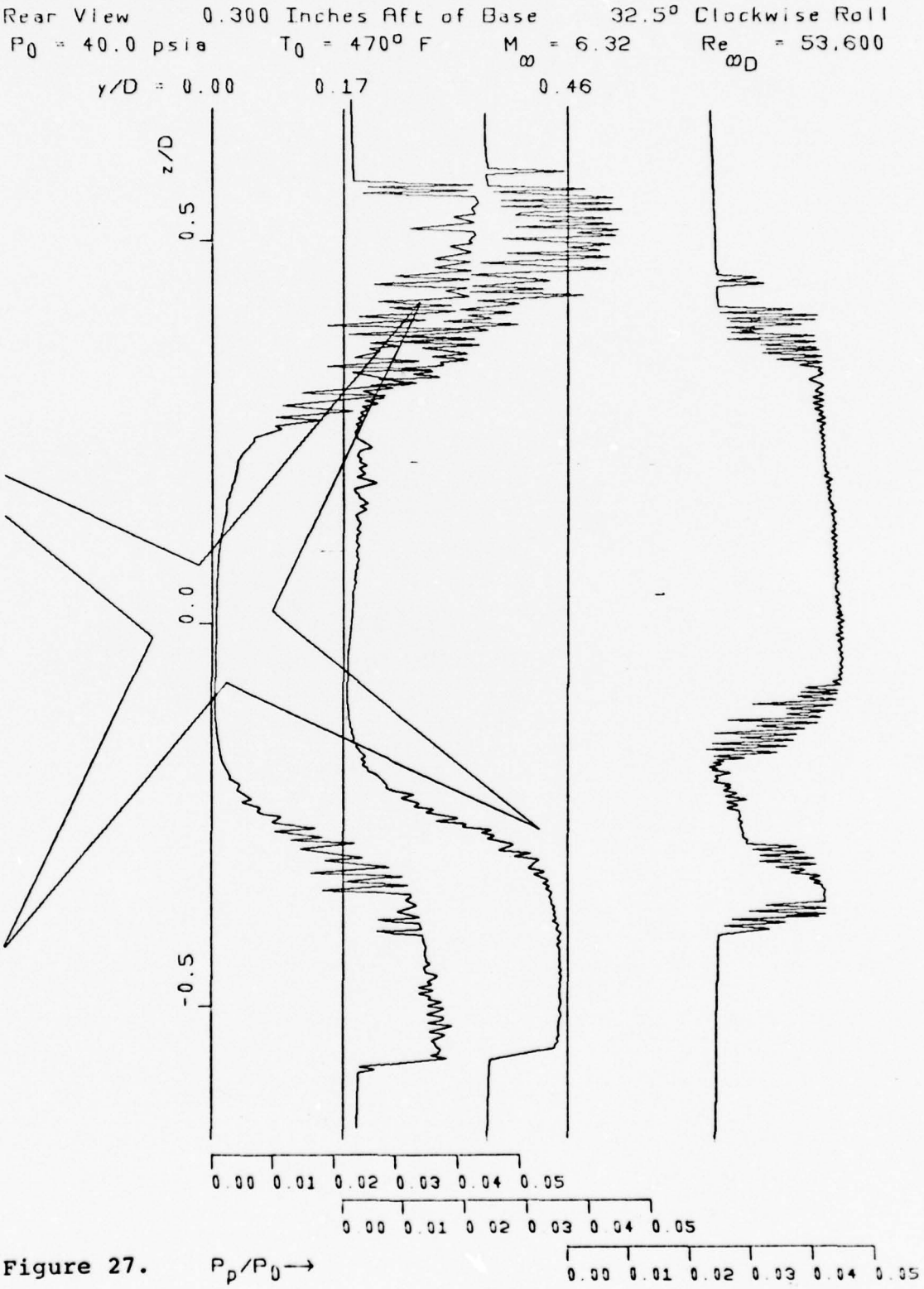

Figure 27. PITOT PRESSURE PROFILES. 15 DEGREE REENTRANT PYRAMID.

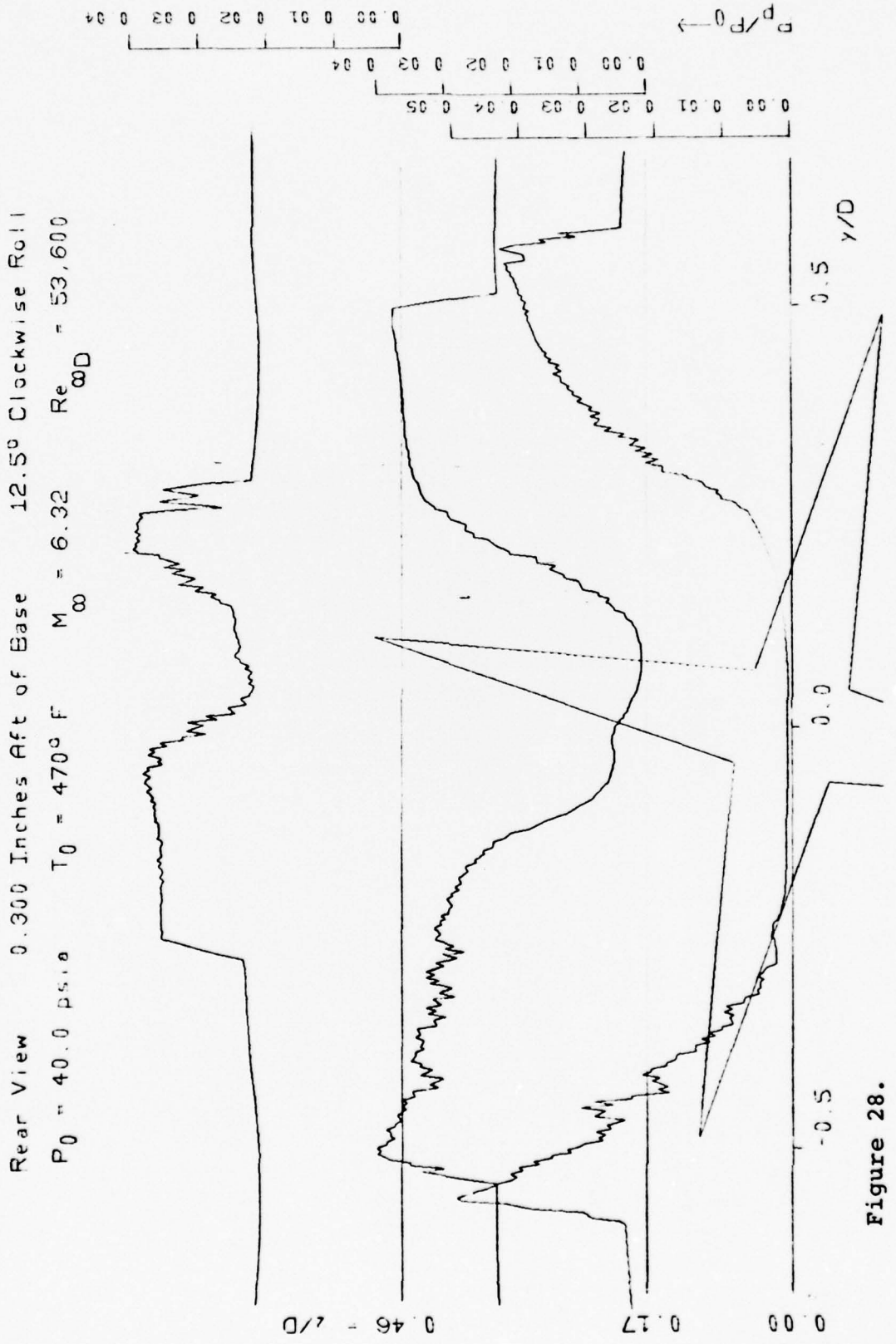

Figure 28.

PITOT PRESSURE PROFILES. 15 DEGREE REENTRANT PYRAMID.

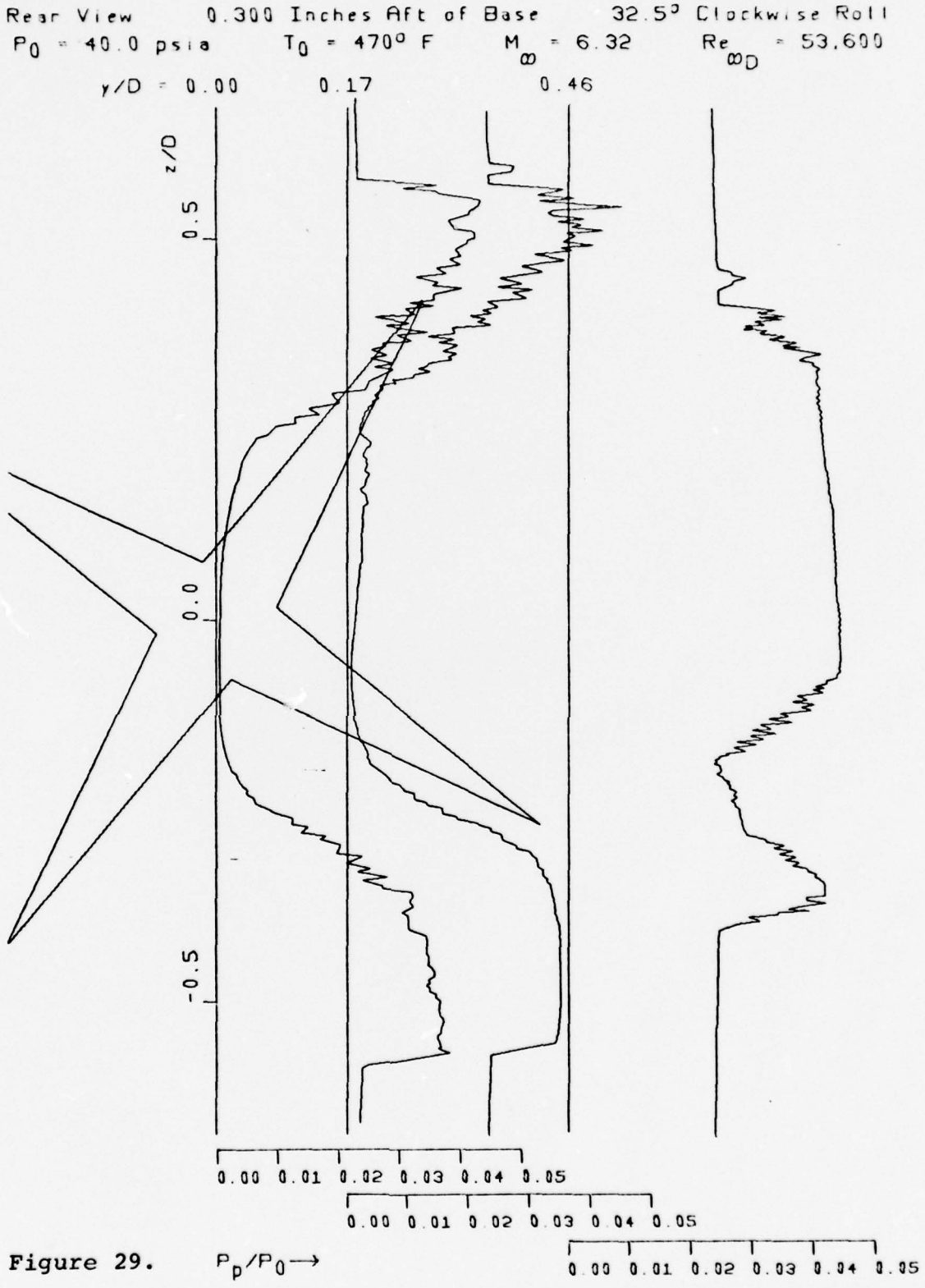

Figure 29. PITOT PRESSURE PROFILES. 15 DEGREE REENTRANT PYRAMID.

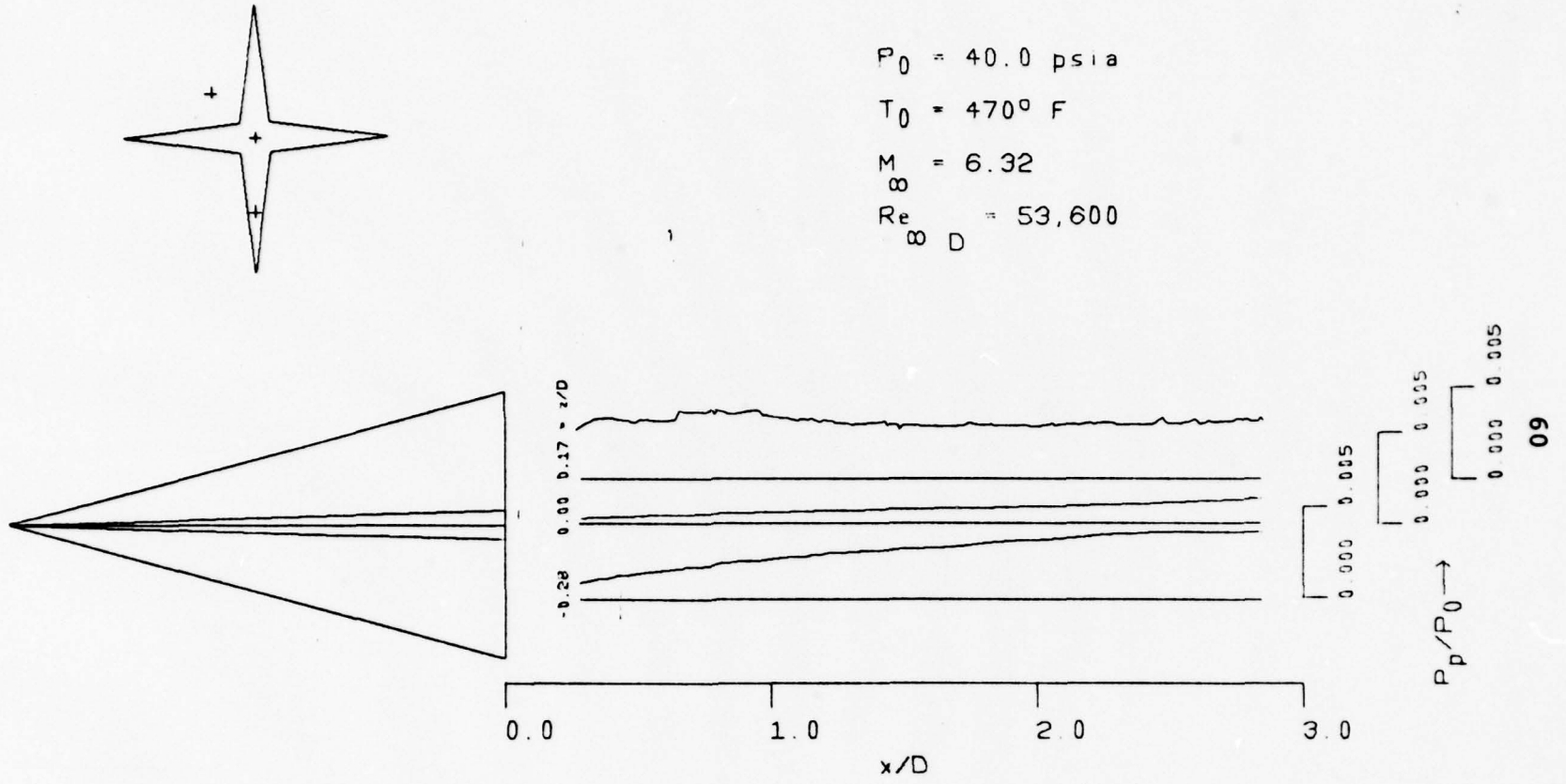

Figure 30.

PITOT PRESSURE PROFILES. 15 DEGREE REENTRANT PYRAMID.

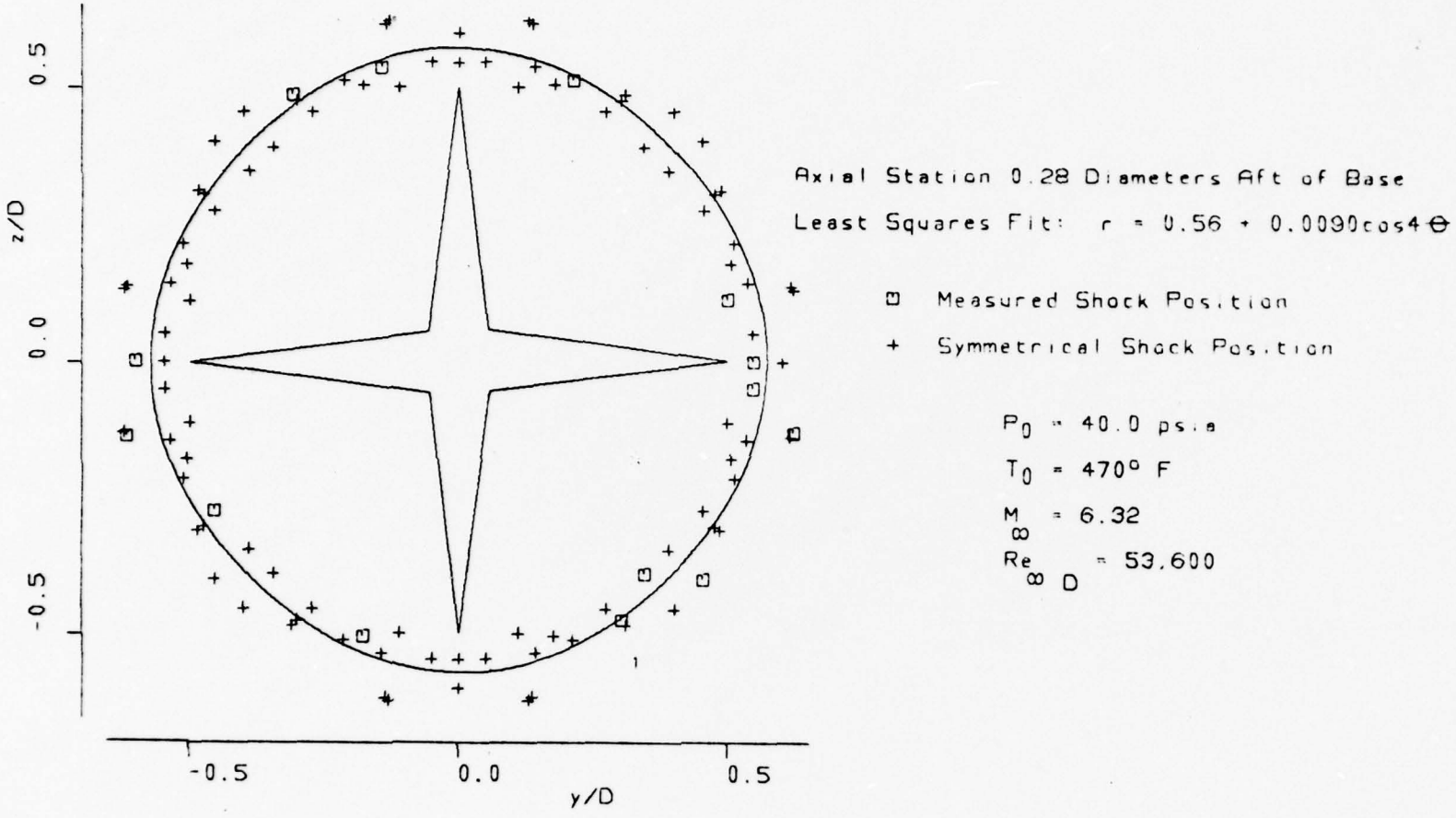

Figure 31. SHOCK TRACE. 15 DEGREE REENTRANT PYRAMID.

profiles positioned using midpoint of viscous core

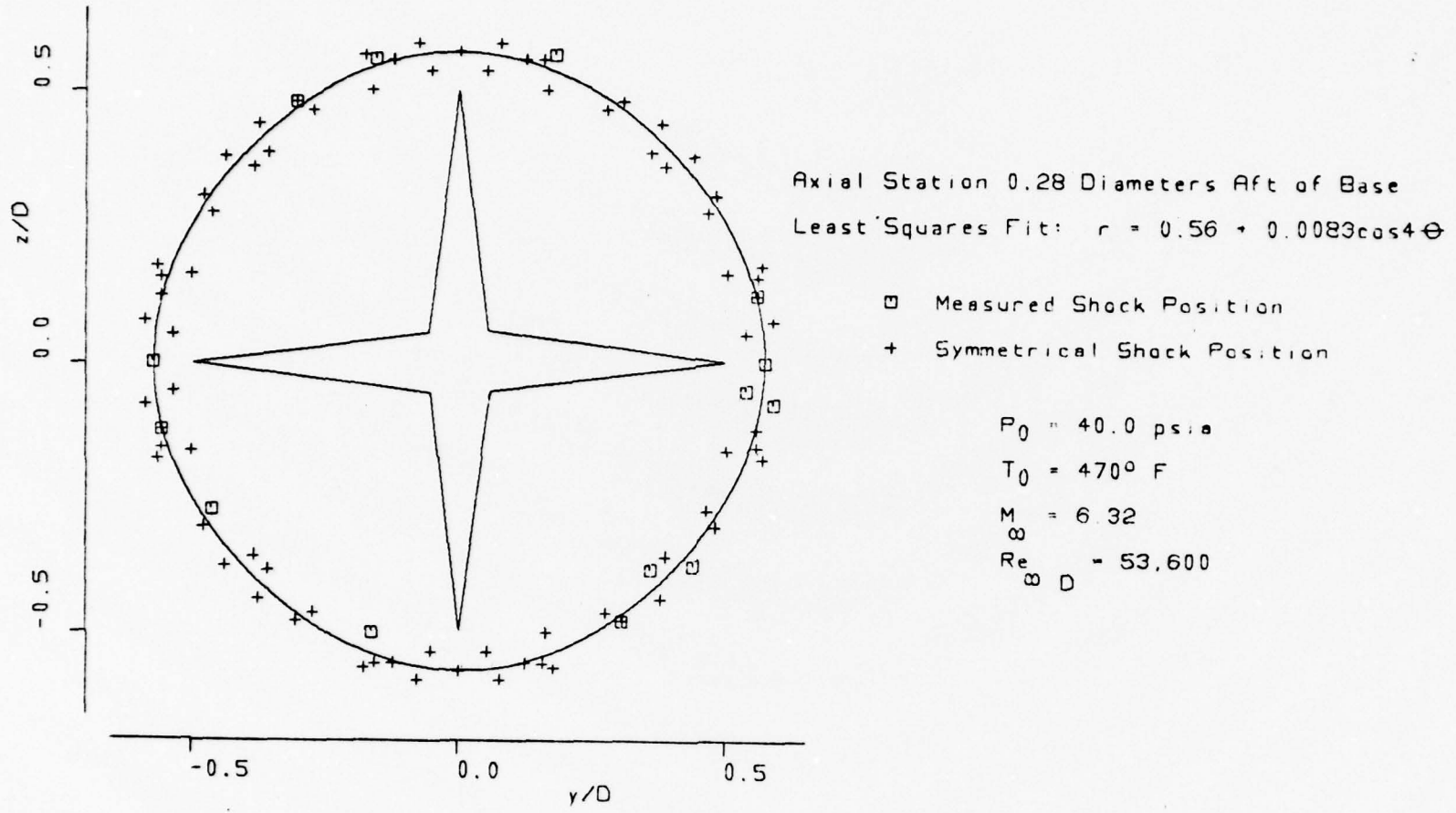

Figure 32. SHOCK TRACE. 15 DEGREE REENTRANT PYRAMID.
profiles positioned using midpoint of bow shocks

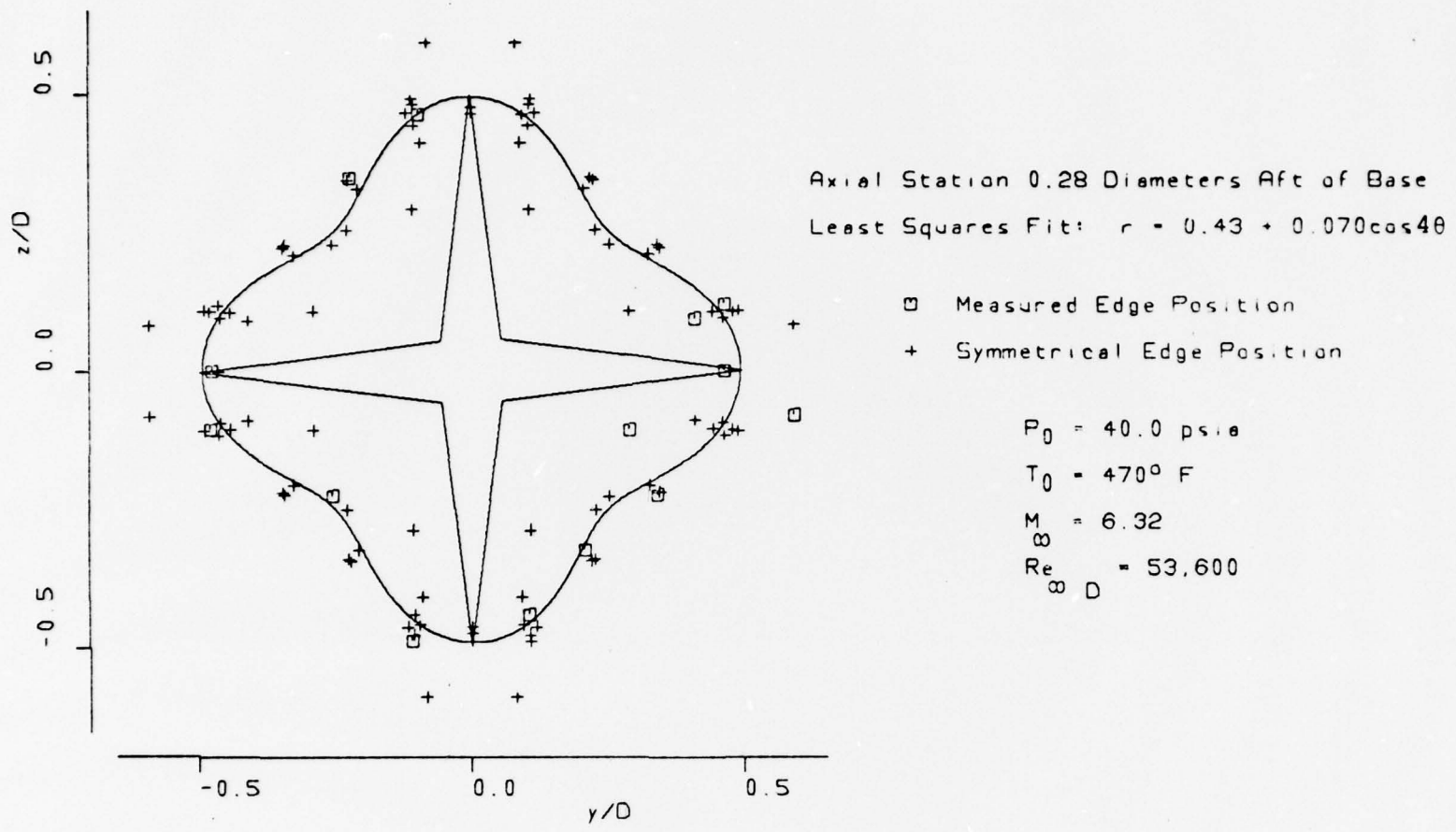

Figure 33. VISCOUS WAKE EDGE. 15 DEGREE REENTRANT PYRAMID.
profiles positioned using midpoint of viscous core

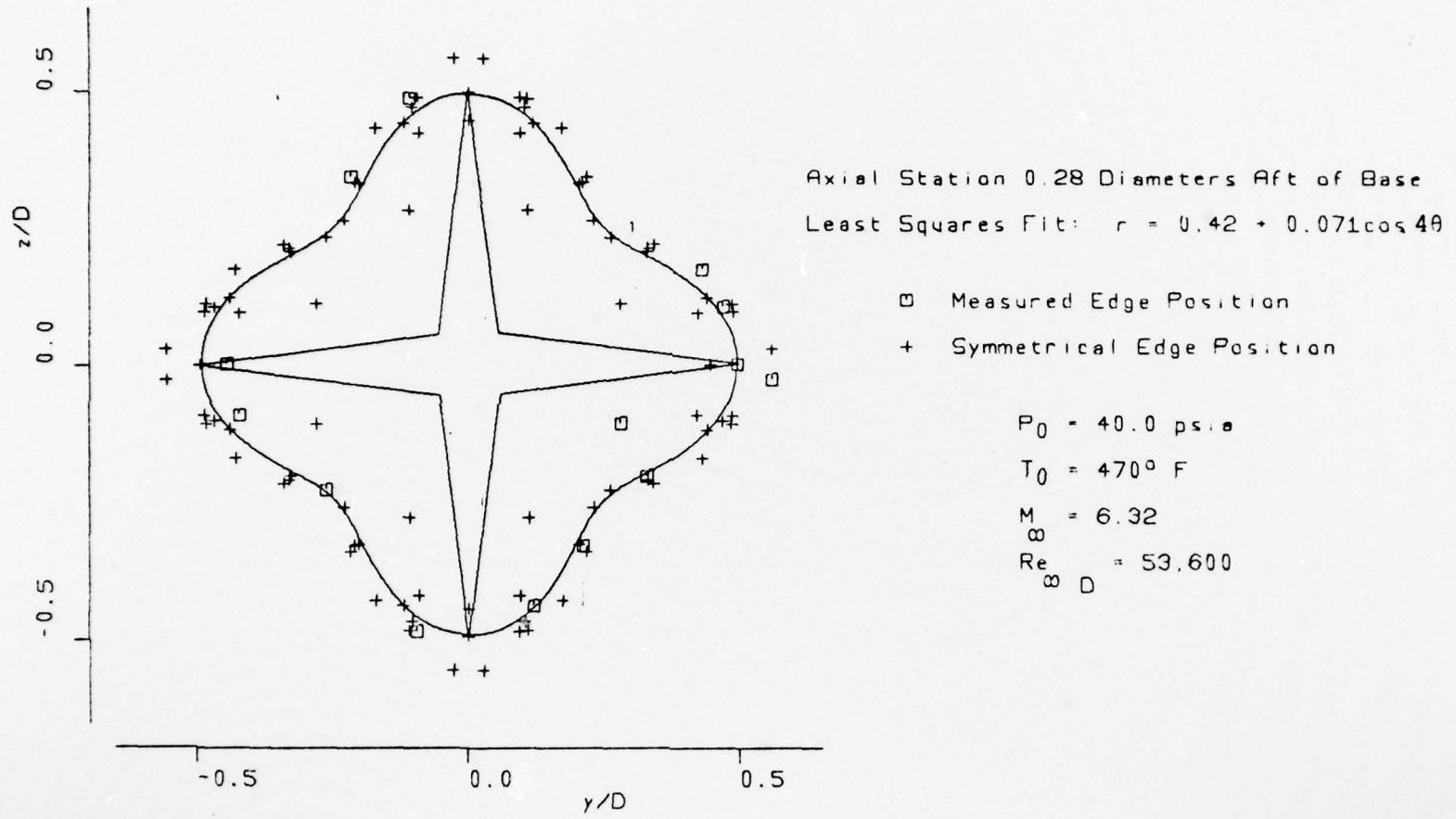

Figure 34. VISCOUS WAKE EDGE. 15 DEGREE REENTRANT PYRAMID.

profiles positioned using midpoint of bow shocks

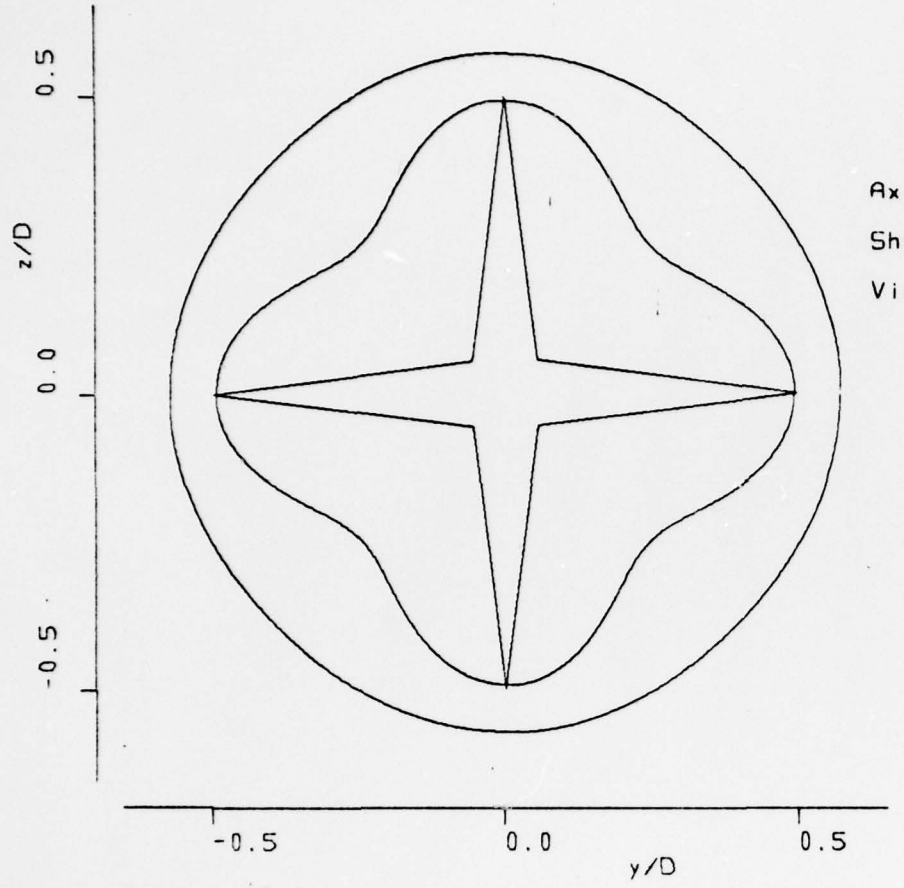

Axial Station 0.28 Diameters Aft of Base

Shock Trace: $r = 0.56 + 0.0083\cos 4\theta$

Viscous Wake Edge: $r = 0.42 + 0.071\cos 4\theta$

$P_0 = 40.0$ psia

$T_0 = 470^\circ$ F

$M_\infty = 6.32$

$Re_{\infty D} = 53,600$

Figure 35.

WAKE CROSS SECTION. 15 DEGREE REENTRANT PYRAMID.

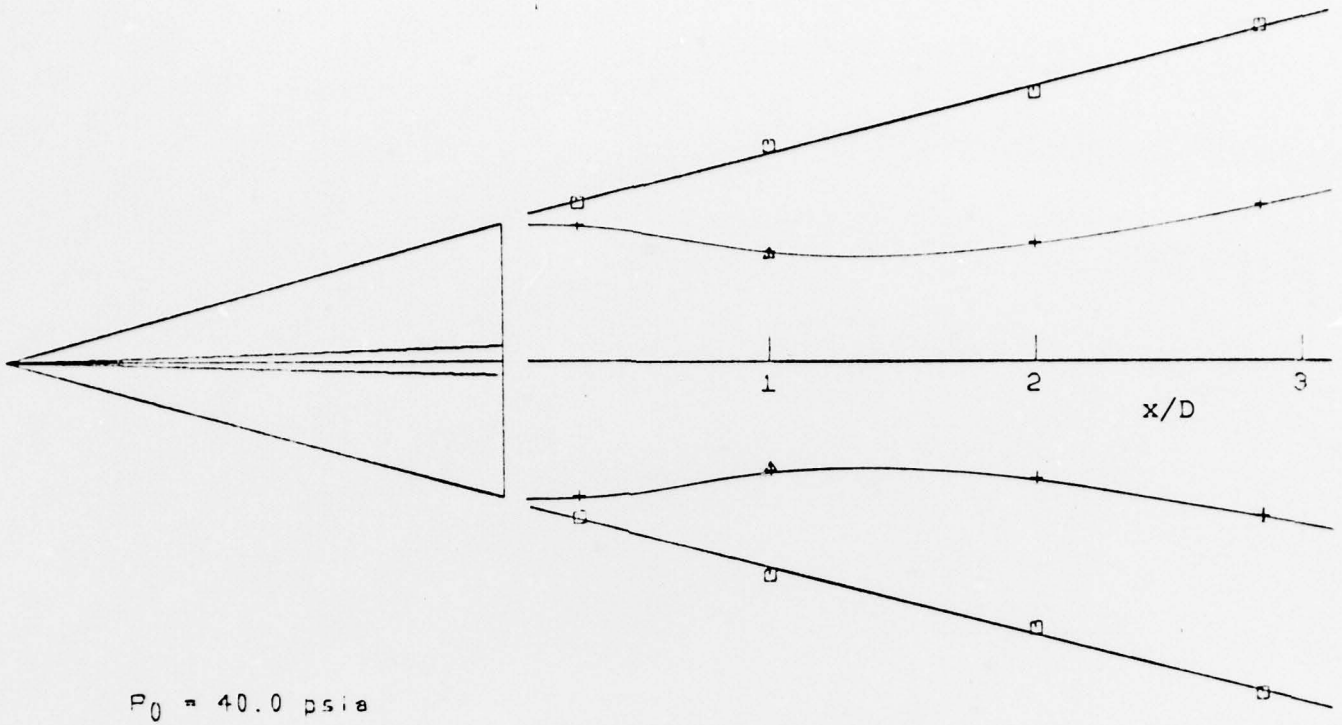

P_0 = 40.0 psia

T_0 = 470° F

M_∞ = 6.32

$Re_{\infty D}$ = 53,600

□ Bow Shock

\+ Viscous Wake Edge

Figure 36.
NEAR WAKE MAP. 15 DEGREE REENTRANT PYRAMID.

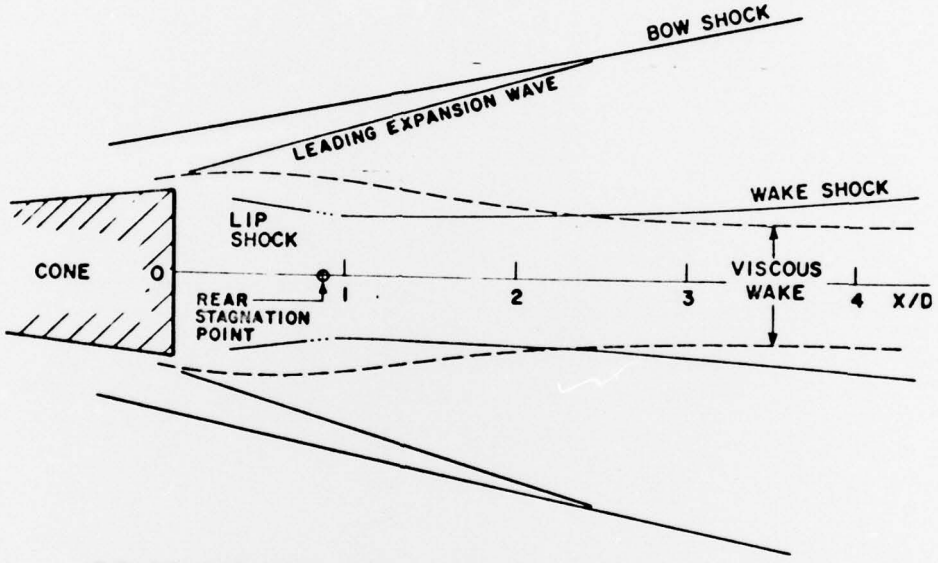

FIG. 37 NEAR WAKE MAP AT Re_{∞_D} = 86,000 (7° CONE AT M_∞ = 6.32)

Figure 38. Drag coefficient vs. Reynolds number at zero angle of attack

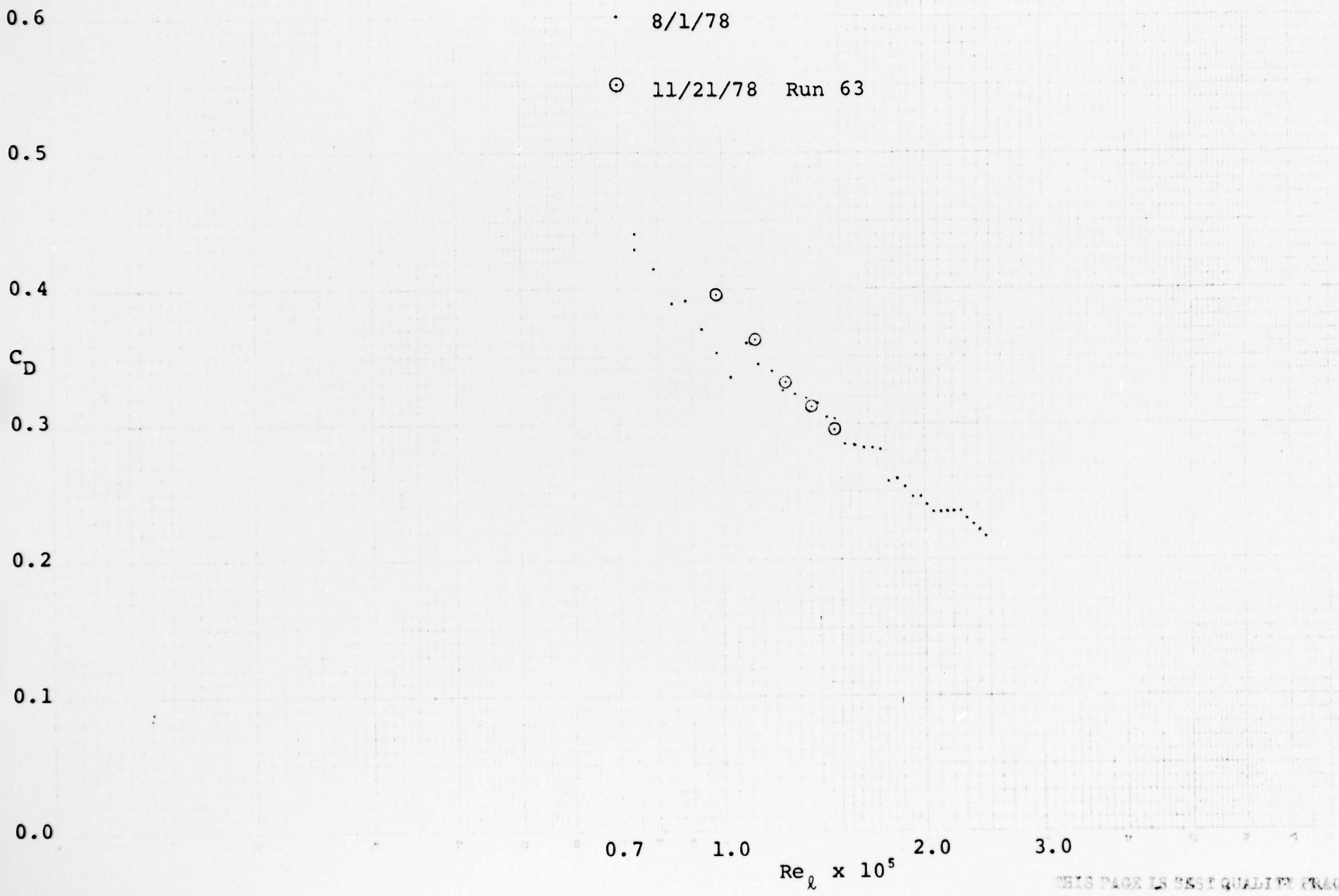

83632 AFOSR - Wake Studies 15° Pyramid [illegible] Pitot Pressure Measurements October 28, 1976 .003" Support Wires

Nominal Wind Tunnel Conditions: Stagnation Pressure = 90 psia, Stagnation Temperature = 470°F, Nozzle Temp. = , $P_{Nozzle} - P_{Bell}$ = .10 mm Hg, Mach No. = 6.3

Run	Type of Traverse (Horizontal, vertical or axial)	Horizontal Station (inches from model ℄)	Vertical Station (inches from model ℄)	Axial Station (inches aft of base)	P_o psia	T_o °F	T_{Noz} °F	$P_{Noz} - P_{Bell}$ mm Hg	Position Axis inches / chart inch	Pressure Axis mm Hg / chart inch	Comments
1	Horizontal		.000	.119	90	470	190	.10	.256	14.40	
2	Vertical	.488		.119	90	470	225	.14	.255	16.05	
3	Vertical	.298		.119	89.3	470	230	.10	.258	16.04	
4	Vertical	.180		.119	82.3	472	237	.128	.255	17.29	
4a	Vertical	.180		.119	89.5	469	241	.128	.255	17.21	Same as Run 4 except for reduced probe drive speed.
5	Vertical	.110		.119	89.6	470	244	.137	.255	17.19	
5a	Vertical	.000		.119	89.5	471	246	.148	.255	17.17	
5b	Horizontal		.000	.119	89.4	469	248	.152	.256	17.25	Same as Run 1. Taken immediately after Run 5a to compare vertical and Horizontal.
6	Horizontal		.180	.119	89.9	470	248	.122	.257	17.27	
7	Axial	.000	.000		89.9	469	248	.10	.373	17.14	
7a	Axial	.000	.000		89.4	470	248	.12	.375	2.68	Same as Run 7 except for higher x-y recorder gain.
7b	Axial	.000	.000					.10	.375	2.66	Same as Run 7 except start at model base in order to include the recirculation region.
8	Axial	.110	.000		89.4	471	250	.11	.374	2.67	
9	Axial	.180	.000		89.6	470	250	.142	.374	5.35	
10	Axial	.298	.000		89.6	470	250	.10	.374	5.35	
11	Axial	.488	.000		89.5	470	250	.10	.374	13.16	
12	Horizontal		-.635		89.5	470	250	.10	.416	13.99	Rear, top, right tungsten wire is broken. Model is at approximately +10° angle of attack.

FORM 20 TECHNOLOGY STORE Transducer Zero Shift: 0 mv = .997 mm Hg Transducer Output slope: -5.362 mm Hg/mv

Table 1. Wake traverses - 0.003 inch diameter wire supported model

83632 AFOSR - Wake Studies 15° Pyramid .005" Support Wires Pitot Pressure Measurements August 26, 1977 & August 30, 1977

Nominal Wind Tunnel Conditions: Stagnation Pressure = 40490 psia, Stagnation Temperature = 470°F, $P_{Nozzle} - P_{Bell} = .10$ mm Hg, Mach No. = 6.3, Probe Speed = 50

Date	Run	Type of Traverse	Horizontal Station (inches from model ℄)	Vertical Station (inches from model ℄)	Axial Station (inches aft of base)	P_o psia	P_{Bell} mm Hg	$P_{Bell_{corrected}}$ mm Hg	T_o °F	T_{Nozzle} °F	$P_{Noz} - P_{Bell}$ mm Hg	Transducer Power Supply volts	Position Axis inches / chart inch	Pressure Axis mm Hg / chart inch	Position Gauge inches / unit	Pressure Axis mv / chart inch	Pressure Axis mm Hg / mv	Bore Pressure mv	M_∞
8/26/77	14	Axial	.000	.000		39.8	1.35	.75	469	143	.111	-6.050	.3577	2.419	.020 / 3.000	-.514	-4.7038	.014350	
	15	Axial	.000	-.110		39.9	1.35	.75	470	148	.110	-6.050	.3573	2.352	.020 / 3.000	-.500	-4.7038	.014350	
	16	Axial	.000	-.180		40.0	1.40	.80	468	153	.100	-6.051	.3573	2.397	.020 / 3.000	-.510	-4.7030	.014352	
	17	Axial	.000	-.298		40.0	1.40	"	468	157	.100	-6.052	.3573	2.357	.020 / 3.000	-.501	-4.7023	.014355	
	18	Axial	-.180	-.180		40.0	1.40	"	469	161	(meter low) .100	-6.053	.3569	2.421	.020 / 3.000	-.515	-4.7015	.014357	
	19	Vertical	.000		.248 = .2856	40.0	1.42	.82	468	170	.090	-6.053	.3354	4.711	-2.200 / .584	-1.002	"	"	
	20	Vertical	.000		.168 = 1.904	39.8	1.45	.85	468	173	.062	-6.053	.3353	6.557	-2.200 / .600	-1.395	"	"	
	21	Vertical	.000		f = .119	39.8	1.40	.80	468	177	(meter low) .100	-6.053	.3346	8.746	-2.200 / .584	-1.860	"	"	6.43
	22	Horizontal		.000	f = .119	40.0	1.45	.85	470	180	.065	-6.053	.3802	8.730	-1.700 / 1.212	-1.857	"	"	
	23	Horizontal		-.180	f = .119	40.0	1.45	.85	470	182	.064	-6.053	.3807	8.788	-1.700 / 1.212	-1.869	"	"	
	24	Horizontal		-.488	f = .119	40.0	1.49	.89	470	183	.065	-6.053	.3807	8.750	-1.700 / 1.212	-1.861	"	"	
	25	Vertical	-.750		.390	39.9	1.49	.89	470	185	.045	-6.053	.3788	8.736	-2.200 / .584	-1.858	"	"	
8/30/77	26	Axial	.000	.000		90.2	2.00	1.40	472	177	.104	-6.043	.3339	2.338	.020 / 3.025	-.496	-4.7093	.014333	
	27	Axial	.000	-.110		90.2	2.20	1.60	470	195	.085	-6.043	.3339	2.357	.020 / 3.025	-.500	"	"	
Broken wire ▼	28	Axial	-.006	-.169		90.5	2.30	1.70	470	205	.067	-6.043	.3328	2.369 (yes) 4.723 (2s)	.032 / 3.037	-.503 (yes) -1.003 (2s)	"	"	
Upper, left, rear wire broke	29	Axial	-.006	-.287		90.5	2.30	1.70	470	217	.088	-6.043	.3328	4.738	.032 / 3.037	-1.006	"	"	
	30	Axial	-.186	-.169		90.5	2.35	1.75	470	223	.065	-6.042	.3335	4.706	.032 / 3.037	-.999	-4.7101	.014331	
	31	Vertical	-.006		2.868	90.0	2.35	"	470	230	(meter low) .100	-6.042	.3335	14.406	-2.189 / .606	-3.059	"	"	
	32	Vertical	-.006		1.916	90.0	2.35	"	470	234	.122	-6.042	.3329	15.836	-2.190 / .606	-3.362	"	"	
	33	Vertical	-.006		.131	90.0	2.15 ?	1.55	468	235	.120	-6.043	.3319	15.779	-2.189 / .606	-3.351	-4.7093	.014333	6.50
	34	Horizontal		.011	.131	90.0	2.35	1.75	470	238	.063	-6.043	.3748	15.796	-1.706 / 1.206	-3.354	-4.7093	.014333	
	35	Horizontal		-.169	.131	90.0	2.25	1.65	470	240	.131	-6.042	.3748	15.820	-1.706 / 1.206	-3.359	-4.7101	.014331	
	36	Horizontal		-.477	.131	90.0	2.25	"	472	240	.100	-6.042	.3743	15.813	-1.706 / 1.206	-3.357	"	"	
	37	Vertical	-.756		.402	90.0	2.25	"	470	241	.100	-6.042	.3442	15.823	-2.159 / .606	-3.359	"	"	

Table 2. Wake traverses - 0.005 inch diameter wire supported model

83632 AFOSR - Wake Studies 15° Pyramid .005" Support Wires Pitot Pressure Measurements August 30, 1977

Nominal Wind Tunnel Conditions : Stagnation Temperature = 470°F, $P_{Nozzle} - P_{Bell} = .10$ mm Hg, Mach No. = 6.3, Probe Speed = 50

Run	Type of Traverse	Horizontal Station (inches from model ℄)	Vertical Station (inches from model ℄)	Axial Station (inches aft of base)	P_o psia	P_{Bell} mm Hg	$P_{Bell_{corrected}}$ mm Hg	T_o °F	T_{Nozzle} °F	$P_{Noz} - P_{Bell}$ mm Hg	Transducer Power Supply volts	Transducer Output mv	Position Axis inches chart inch	Pressure Axis mm Hg chart inch	Position Range inches inches	Pitot Pressure mm Hg	P_∞ mm Hg	P_o/P_∞	Re_δ	$\frac{1}{\sqrt{Re_\delta}}$
38	Stationary	-.006	.011	.062	90.0	2.33	1.73	468	242	.100 (meter low)	-6.041	-.509				2.47	2.19	1.13	2.25×10^5	$.445 \times 10^{-2}$
					80.0	2.11	1.51	464	243	.100 low	-6.041	-.477				2.31	1.95	1.19	2.0×10^5	$.472 \times 10^{-2}$
					70.1	1.99	1.39	470	242	.100 low	-6.041	-.447				2.17	1.70	1.27	1.75×10^5	$.505 \times 10^{-2}$
					60.0	1.85	1.25	470	240	.100 low	-6.041	-.427				2.05	1.46	1.43	1.5×10^5	$.595 \times 10^{-2}$
					50.0	1.70	1.10	470	237	.100	-6.041	-.381				1.86	1.22	1.53	1.25×10^5	$.598 \times 10^{-2}$
					40.0	1.65	1.05	470	231	.031	-6.041	-.362				1.77	.973	1.82	1.0×10^5	$.568 \times 10^{-2}$
					30.0	1.65	1.05	470	228	.083	-6.041	-.374				1.83	.730	2.51	7.5×10^4	$.771 \times 10^{-2}$
39	Vertical	-.186		.131	40.1	1.65	1.05	470	221	.035	-6.042		.3442	15.845	-2.189 .606					
40	Vertical	.174		.131	40.0	1.60	1.00	470	216	.039	-6.042		.3672	15.809	-2.196 .606	Spike in data due to disconnection of BPM from circuit. Run repeated as run 41				
41	Vertical	.174		.131	40.0	1.58	.98	470	211	.042	-6.042		.3673	15.814	-2.189 .606	Same as Run 40.				

	Pressure Axis inches chart inch	Pressure Axis mm Hg mv	Zero Pressure mv
39	-3.364	-4.7101	.019331
40	-3.356	"	"
41	-3.358	"	"

FORM 20 TECHNOLOGY STORE

Table 3. Base pressure and wake traverses - 0.005 inch diameter wire supported model

83632 AFOSR - Wake Studies 15° Pyramid Pitot Pressure Measurements August 11, 1978 Magnetically Suspended Permanent Magnet Model

Nominal Wind Tunnel Conditions: Stagnation Pressure = 40, 90 psia ; Stagnation Temperature = 470°F ; $P_{Nozzle} - P_{Bell} = 0.10$ mm Hg ; Mach No. = 6.3

	Date	Run	Type of Traverse	Horizontal Station (inches from model ℄)	Vertical Station (inches from model ℄)	Axial Station (inches aft of face)	P_o psia	P_{Bell} mm Hg	T_o °F	T_{Nozzle} °F	$P_{Noz} - P_{Bell}$ mm Hg	Probe Speed	Transducer Power Supply volts	Roll Angle degrees cw looking from rear	Position Axis inches chart inch	Position Range inches inches	Pressure Axis mv chart inch	Pressure Axis mm Hg mv	Pressure Axis mm Hg chart inch		
	8/11/78	42	Horizontal		.000	.000	89.7	2.15	470	140	0.10	70			0.4162	-1.70 2.00	-1.823	-4.723	8.609		
FREE JET	8/11/78	43	Horizontal		.000	.000	39.9	1.75	480	168	-0.04	65	-6.032		0.4387	-1.90 2.00	-1.000	-4.723	4.723	0.ffset at	9.5"
	8/11/78	43a	Horizontal		.000	.000	39.6	1.70	473	190	-0.066	65			0.4341	-1.70 2.00	-1.000	-4.723	4.723	0.ffset at	8.5"
	8/11/78	44	Vertical	.000		.000	40.0	1.65	467	160	-0.06	65			0.2553	-1.48 1.10	-1.000	-4.723	4.723		4.5
P_o = 40	11/3/78	45	Horizontal		-.488	.300	40.4	1.50	420	151	-0.042	55		10 to 15	0.3759	-1.70 1.90	-2.367	-4.717	11.165		
	11/3/78	46	Horizontal		-.180	.300	40.4	1.48	455	156	-0.039	55			0.3753	-1.70 1.90	-2.319	-4.717	10.936		
	11/3/78	47	Horizontal		.000	.300	40.0	1.50	466	163	-0.035	55	-6.040		0.3762	-1.70 1.90	-2.376	-4.717	11.205		
	11/3/78	48	Vertical	.000		.300	40.2	1.50	470	178		55			0.4112	-1.70 1.05	-2.371	-4.717	11.186		
	11/3/78	49	Vertical	.180		.300	40.0	1.68	470	187		55		25 to 40	0.4106	-1.70 1.05	-2.378	-4.717	11.218		
	11/3/78	50	Vertical	.488		.300								25 to 40	0.4106	-1.70 1.05	-2.378	-4.717	11.217		
	11/3/78	51	Vertical	.000		1.07	40.5	1.54	470	163	-0.15	55		5	0.4092	-1.70 1.05	-2.369	-4.717	11.172	New Model	
	11/9/78	52	Vertical	.000		2.14	40.4	1.40	468	119	-0.082	55	-6.039	0	0.4112	-1.76 0.99	-2.362	-4.718	11.144	Abs. Press	
	11/9/78	53	Vertical	.000		3.05	40.5	1.40	431	116	0.089	55		0	0.4113	-1.76 0.99	-2.367	-4.718	11.165	Abs. Press	
		54	Axial	.000	-.488																
	11/9/78	55	Axial	.000	-.298		40.2	1.50	461	136	0.010	55		0	0.4846	0.30 3.05	-2.379 -0.4934	-4.720 -4.720	11.228 2.329		
		56	Axial	.000	-.180																
		57	Axial	.000	-.110																
	11/9/78	58	Axial	.000	.000		39.8	1.50	470	143	-0.062	55		0	0.4844	0.30 3.05	-0.5000	-4.720	2.360		
	11/9/78	59	Axial	-.180	-.180		39.8	1.58	470	146	-0.086	55	-6.036	0	0.4852	0.28 3.05	-0.9933	-4.720	4.688		
	8/22/78	60	Horizontal		.000	.300	40.4	1.80	475	148	-0.01	65	-6.038	0	0.4184	-1.70 1.97	-1.000	-4.718	4.718	Probe Diff. Leak	
	8/31/78	61	Horizontal		-.488	.300	40.0	8.0	448	160	-0.8	65	-6.073	45	0.4213	-1.70 1.90	-2.009	-4.691	9.420	Subsonic	

FORM 20 TECHNOLOGY STORE

Table 4. Wake traverses - magnetically suspended model

83632 AFOSR - Wake Studies 15° Pyramid Pitot Pressure and Drag Measurements November 21, 1978 Magnetically Suspended Armament Magnet Model

Nominal Wind Tunnel Conditions: Stagnation Temperature = 470 °F, $P_{Nozzle} - P_{Bell} = 0.10$ mm Hg, Mach No. = 6.3

Date	Run	Type of Traverse	Horizontal Station (inches from model ℄)	Vertical Station (inches from model ℄)	Axial Station (inches aft of base)	P_o psia	P_{Bell} mm Hg	T_o °F	T_{Nozzle} °F	$P_{Noz} - P_{Bell}$ mm Hg	Transducer Output mv	Pitot Pressure mm Hg	P_∞ mm Hg	P_∞ / P_o	Re_∞ $\cdot 10^5$	$\frac{1}{T Re_{\delta/2}}$	Drag Shunt mv	Drag Current amperes	Drag Force ounces	Drag Bias Shunt mv	Drag Bias amps
11/9/78	G2	Stationary	.000	.000	.300	40	1.6	470	156		-0.162	0.537	0.973	0.552	1.01	0.0668	2.54	10.16	0.461	37.30	14.92
						45									1.14	0.0629	2.62	10.48	0.492	37.30	14.92
						Model Absolute Positioned: Roll = 0°															
11/21/78	G3	Stationary	.000	.000	.300	39.8	1.42	470	116		-0.153	0.495	0.968	0.511	1.01	0.0668	2.42	9.68	0.417	37.66	15.064
						45.5	1.49	485	119		-0.159	0.523	1.107	0.472	1.15	0.0626	2.47	9.88	0.435	37.59	15.036
						50.4	1.53	474	122		-0.165	0.551	1.226	0.449	1.28	0.0593	2.49	9.96	0.442	37.64	15.056
						55.4	1.59	474	130		-0.183	0.636	1.347	0.472	1.40	0.0567	2.53	10.12	0.457	37.59	15.036
						60.0	1.64	490	133	0.128	-0.197	0.702	1.459	0.481	1.52	0.0544	2.56	10.24	0.470	37.61	15.044

Table 5. Base pressure and drag - magnetically suspended model

83G32 AFOSR - Wake Studies 15° Pyramid Force Data (DVM) Magnetically Suspended Permanent Magnet Model

Nominal Wind Tunnel Conditions: Stagnation Temperature = 470°F, $P_{Nozzle} - P_{Bell} = 0.10$ mm Hg, Mach No. = 6.3

Date	Run	P_o psia	$Re_f \cdot 10^6$	L1-L2 mv	L1+L2 mv	L3 mv	L4 mv	Drag mv	Drag Bias mv	L1 amp	L2 amp	L3 amp	L4 amp	Drag amp	Drag Bias amp	Drag Force ounces	Abs Pos just before run ✓	Roll degrees cw looking from rear	C_D based on base area	Nozzle M_∞ & Re_f (1/in) $\cdot 10^6$
8/14/78		Wind Off		-0.96	3.07	-139.2	-88.7	1.02	11.04	22.64	26.48	-2.78	-1.77	4.08		-0.045				Stop In, Re 0.74 M 7 psi
				-0.96	3.11	-112.1	-105.0	1.00	10.97	21.04	28.72	-2.24	-2.10	4.00		-0.050				Stop In, Re 0.74 M 6 psi
		30	0.76	-0.97	2.66	95.1	445.3	2.19	9.29	17.40	25.16	1.40	8.91	8.76		0.335		45°	0.422	0.74
8/17/78		30	0.76	-0.86	2.68	-5.6	105.7	2.21	35.86	18.00	24.88	-0.11	2.11	8.84	14.34	0.342		45°	0.431	0.74
		30	0.76	-0.85	2.70	-41.1	30.1	2.24	35.86	18.20	25.00	-0.82	0.60	8.96	14.34	0.351		45°	0.442	0.74
		32	0.81	-0.86	2.74	-66.6	-29.4	2.27	35.81	18.48	25.36	-1.33	-0.59	9.08	14.32	0.362		45°	0.428	0.79
		34	0.86	-0.85	2.72	-56.8	-7.9	2.29	35.81	18.36	25.16	-1.14	-0.16	9.16	14.32	0.369		45°	0.410	0.84
		36	0.91	-0.69	2.47	-21.3	62.2	2.30	35.77	17.00	22.52	-0.41	1.24	9.20	14.31	0.373			0.392	Start to roll reversed 0.88
		38	0.96	-0.63	2.34	45.3	188.2	2.31	35.87	16.20	21.24	0.91	3.76	9.24	14.35	0.376		10°	0.374	0.93
8/22/78		30	0.76	-0.95	2.50	361.3	1032.9	2.31	35.88	16.20	23.80	7.23	20.66	9.24	14.35	0.376			0.474	0.74
		30	0.76	-0.74	2.22	417.9	1162.1	2.32	35.87	14.80	20.72	8.36	23.24	9.28	14.35	0.380			0.479	0.74
		40	1.01	-0.56	2.05	318.0	743.4	2.32	35.76	14.16	18.64	6.36	14.87	9.28	14.30	0.380			0.469	0.98
		40	1.01	-0.53	2.03	315.4	727.0	2.32	35.69	14.12	18.36	6.31	14.54	9.28	14.28	0.380			0.459	0.98
8/31/78		40	1.01	-0.86	3.00	-103.5	-67.7	1.09	36.25	20.56	27.44	-2.07	-1.35	4.36	14.50	-0.023		45°		Subsonic 0.98
11/3/78	51	40.5	1.03	-0.70	2.46	66.1	186.6	2.48	37.22	16.38	22.48	1.32	3.73	9.92	14.89	0.439		0	0.410	1.00
11/9/78	52	40.4	1.02	-0.69	2.44	-28.5	32.9	2.44	37.68	16.76	22.28	-0.57	0.66	9.76	15.07	0.423	✓	0	0.396	0.99
	53	40.5	1.03	-0.63	2.33	40.1	175.2	2.39	37.55	16.12	21.16	0.80	3.50	9.56	15.02	0.406	✓	0	0.379	1.00
	55	40.2	1.02	-0.66	2.43	-31.7	41.6	2.49	37.38	16.80	22.08	-0.63	0.83	9.96	14.95	0.441		0	0.415	0.99
	58	39.8	1.01	-0.69	2.49	-42.9	13.9	2.51	37.36	17.16	22.68	-0.86	0.28	10.04	14.94	0.451		0	0.428	0.98
	59	39.8	1.01	-0.67	2.48	-59.1	-18.2	2.53	37.30	17.16	22.52	-1.18	-0.36	10.12	14.92	0.458		0	0.435	0.98
	62	40	1.01	-0.66	2.48	-62.8	-22.3	2.54	37.30	17.20	22.48	-1.26	-0.45	10.16	14.92	0.461			0.436	0.98
	62	45	1.14	-0.65	2.50	-101.6	-94.3	2.62	37.30	17.40	22.60	-2.03	-1.89	10.48	14.92	0.493			0.464	1.11
11/21/78	63	39.8	1.01	-0.73	2.46	79.8	240.1	2.42	37.66	16.76	22.60	1.60	4.80	9.68	15.06	0.417	✓	0	0.396	0.98
	63	45.5	1.15	-0.69	2.47	61.1	212.2	2.47	37.59	17.00	22.52	1.22	4.24	9.88	15.09	0.436		0	0.362	1.13
	63	50.4	1.28	-0.73	2.56	83.7	253.5	2.49	37.64	17.56	23.40	1.67	5.07	9.96	15.06	0.441		0	0.331	1.24
	63	55.4	1.40	-0.71	2.57	89.4	266.9	2.53	37.59	17.72	23.40	1.80	5.34	10.12	15.04	0.458		0	0.313	1.36
	63	60.0	1.52	-0.72	2.59	102.5	292.5	2.56	37.61	17.84	23.60	2.05	5.85	10.24	15.04	0.469		0	0.296	1.47

FORM 20 TECHNOLOGY STORE

Table 6. Drag coefficient vs. Reynolds number

83632 AFOSR-Wake Studies 15° Pyramid Force Data (Panel Meters) Magnetically Suspended Permanent Magnet Model

Nominal Wind Tunnel Conditions: Stagnation Temperature = 470°F, $P_{Nozzle} - P_{Bell} = 0.10$ mm Hg, Mach No. = 6.3, Model Not Absolute Positioned

Date	Run	P_o psia	Re_l $\times 10^6$	L1 amps	L2 amps	L3 amps	L4 amps	Drag amps	Drag Force ounces	Adjust Model Position Just Before Run ✓	Roll degrees cw looking from rear	C_D based on base area		Re_l (1/in) $\times 10^6$	
7/31/78		30	0.76	8.0	11.5	-2.0	0	9.5	0.372			0.469		0.74	
		30	0.76	8.5	12.0	-2.0	0	9.5	0.372			0.469		0.74	
		30	0.76	8.0	11.2	-2.0	0	9.5	0.372			0.469		0.74	
		32	0.81	8.0	11.2	-2.0	0	9.8	0.400			0.473		0.79	
8/1/78		0		9.2	13.1	-3.0	-0.5	4.25	-0.039		45		Sting In		
		30	0.76	7.0	9.6	2.0	7.0	9.12	0.340		45	0.429		0.74	
		30	0.76	8.0	11.5	1.0	5.5	9.25	0.350		45	0.441		0.74	
		32	0.81	7.8	11.2	1.0	6.0	9.25	0.350		45	0.414		0.79	
		34	0.86	7.5	10.6	2.0	7.0	9.25	0.350		45	0.389		0.84	
		36	0.91	7.9	11.5	1.0	5.5	9.50	0.372			0.391	Start to roll vertical	0.88	
		38	0.96	7.4	10.2	2.0	8.0	9.50	0.372		0	0.370		0.93	
		40	1.01	7.2	10.2	2.5	8.5	9.50	0.372		0	0.352		0.98	
		42	1.06	7.2	10.2	2.5	8.5	9.50	0.372		0	0.335		1.03	
		44	1.11	7.5	10.5	-0.5	2.5	10.00	0.419		0	0.360		1.08	
		46	1.17	7.5	10.5	-0.5	2.5	10.00	0.419		0	0.344		1.13	
		48	1.22	7.5	10.5	-0.5	2.5	10.12	0.430		0	0.339		1.18	
		50	1.27	7.5	10.4	-0.5	2.5	10.12	0.430		0	0.325		1.23	
		52	1.32	7.5	10.5	-1.0	2.5	10.25	0.443		0	0.322		1.28	
		54	1.37	7.5	10.4	-1.0	2.5	10.38	0.456		0	0.319		1.33	
		56	1.42	7.5	10.5	-1.0	2.0	10.50	0.468		0	0.316		1.38	
		58	1.47	7.5	10.4	-1.5	2.0	10.50	0.468		0	0.305		1.43	
		60	1.52	7.5	10.4	-1.5	2.0	10.50	0.468		0	0.295		1.47	
		62	1.57	7.5	10.4	-1.5	2.0	10.50	0.468		0	0.285		1.52	
		64	1.62	7.5	10.4	-1.5	2.0	10.62	0.480		0	0.284		1.57	
		66	1.67	7.6	10.5	-1.5	2.0	10.75	0.492		0	0.282		1.62	
		68	1.72	7.6	10.4	-2.0	1.5	10.88	0.507		0	0.282		1.67	
		70	1.77	7.6	10.4	-2.0	1.0	11.00	0.520		0	0.291		1.72	
		60	1.52	7.5	10.2	-2.0	1.5	10.62	0.480		0	0.302		1.47	probably due to low flow. Re range is wrong
		70	1.77	7.5	10.2	-2.5	0.5	11.00	0.520		0	0.281		1.72	
		72	1.82	7.4	10.0	0.0	4.5	10.75	0.492	✓	0	0.258		1.77	
		74	1.87	7.2	10.0	0.5	5.0	10.88	0.507		0	0.259		1.82	
		76	1.93	7.2	10.0	0.5	5.0	10.88	0.507		0	0.252		1.87	
		78	1.98	7.2	9.9	0.5	5.5	10.88	0.507		0	0.246		1.92	
		80	2.03	7.2	9.8	1.0	6.0	11.00	0.520		0	0.246		1.97	
		82	2.08	7.1	9.8	1.0	6.0	11.00	0.520		0	0.240		2.01	
		84	2.13	7.1	9.8	0.5	5.5	11.00	0.520		0	0.234		2.06	
		86	2.18	7.1	9.8	0.5	5.5	11.12	0.532		0	0.234		2.11	
		88	2.23	7.2	9.9	0.5	5.5	11.25	0.545		0	0.234		2.16	
		90	2.28	7.0	9.6	0.5	5.5	11.38	0.560		0	0.235		2.21	
		92	2.33	7.0	9.5	0.5	5.0	11.50	0.573		0	0.236		2.26	
		94	2.38	7.0	9.5	1.0	6.0	11.50	0.573	✓	0	0.230		2.31	
		96	2.43	6.9	9.4	2.0	7.5	11.50	0.573		0	0.226		2.36	
		98	2.48	6.9	9.4	2.5	8.0	11.50	0.573		0	0.221		2.41	
		100	2.53	6.9	9.2	2.5	8.5	11.50	0.573		0	0.217		2.46	
8/22/78	GO	40	1.01	6.0	8.2	5.0	12.0	9.75	0.395			0.373		0.98	
11/3/78		40	1.01	8.2	11.5	-2.5	-2.0	10.50	0.468			0.442		0.98	
	51	40	1.01	7.2	10.0	0.5	3.5	10.25	0.443			0.419		0.93	

FORM 20 TECHNOLOGY STORE

Table 7. Drag coefficient vs. Reynolds number

REFERENCES

1. McLaughlin, D K, "Experimental Investigation of the Mean Flow and Stability of the Laminar Supersonic Cone Wake", AFOSR Scientific Report, AFOSR 70-0072TR, January, 1970 (also Ph.D. Thesis, MIT, Cambridge, Ma., November, 1969).

2. Blankson, I M, "Experimental Study of the Mean Flow in a Laminar Axisymmetric Cone Near Wake at M_∞ = 6.3 using Magnetic Model Suspension", Ph.D. Thesis, MIT, Cambridge, Ma., June, 1973.

3. Maikapar, G I, "On the Wave Drag of Non-Axisymmetric Bodies at Supersonic Speeds", Journal of Applied Mathematics and Mechanics (PMM), Vol 23, No. 2, 1959, pp 528-531.

4. Seddon, J and A Spence, "The Use of Known Flow Fields as an Approach to the Design of High Speed Aircraft", AGARD CP-30, Paper #10, May, 1968.

5. Finston, M and M Solomon, "Wake Studies Related to Reentrant Pyramids", Interim Scientific Report, AFOSR Contract F44620-76-C-0049, February, 1977.

6. Solomon, M, M Finston and C W Haldeman, "Wake Studies Related to Reentrant Pyramids", Interim Scientific Report, AFOSR Contract F44620-76-C-0049, February, 1978.

7. Tilton, E L, III, et al., "The Design and Initial Operation of a Magnetic Model Suspension and Force Measurement System", ARL Report 63-16, Wright-Patterson Air Force Base, Ohio, August, 1962. (Also, MIT Aerophysics Laboratory TR 22, August, 1962.)

8. Covert, E E and E L Tilton, III, "Calibration of a Magnetic Balance System for Drag, Lift and Pitching Moment", MIT Aerophysics Laboratory, Cambridge, Ma., May, 1963.

9. Ames Research Staff, "Equations, Tables and Charts for Compressible Flow", NACA Report 1135, 1953.

10. Finston, M, "Progress Report - September, 1978 through November, 1978", AFOSR Contract F44620-76-C-0049, March, 1979.

11. Martellucci, A, et al., "Measurements of the Turbulent Near Wake of a Cone at Mach 6", AIAA 3d Aerospace Sciences Meeting, New York, January 24-26, 1966.

12. Cassanto, J J, N S Rasmussen and J D Coats, "Correlation of Measured Free Flight Base Pressure Data for M=4 to M=19 in Laminar and Turbulent Flow", AIAA Paper No. 68-699, June, 1968.

LIST OF SYMBOLS

C_D	drag coefficient at zero angle of attack
D	reentrant pyramid model base diameter (external rib span)
ℓ_r	length of recirculation region
M	Mach number
P_o	free stream stagnation pressure
P_B	base pressure
P_P	Pitot pressure
Re	Reynolds number
$Re_{\infty D}$	free stream Reynolds number based on base diameter
$Re_{\infty \ell}$	free stream Reynolds number based on model length
S_i	internal rib span
T_o	free stream stagnation temperature
X	axial coordinate
Y	horizontal coordinate
Z	vertical coordinate
χ	hypersonic viscous interaction parameter $= M^3/\sqrt{Re_\ell}$

Subscripts

$(\ )_o$	stagnation condition of fluid (isentropic)
$(\ )_{design}$	design point of reentrant pyramid
$(\ )_p$	pitot
$(\ )_\infty$	free stream condition